Reply to referee's comments

Dear editor,

We thank your and the reviewer's time for constructing the comments.

In the following, we have addressed all the comments, with the original review text underlined in italics and red.

Line 17: "p-coupled" and "p-fixed" are not generally known terms. They should not be used without explicit definition. Please consider rephrasing, e.g.: In addition to the fully coupled implementation of the scavenging behaviour of 231Pa and 230Th with the active marine ecosystem module (p-coupled), another form of 231Pa and 230Th scavenging have also been implemented with prescribed particle flux fields of the present climate (p-fixed).

Thanks for this advice. We have rephrased as suggested (line 17-20).

Line 96: Please explain in more detail: how can the effects of circulation on 231Pa/230Th be separated from the effects of particle fluxes simply by using two different non-confirmed particle schemes?

We have modified the text to make it clearer. For p-fixed Pa/Th, the particle flux is fixed at present values and the only thing affect p-fixed Pa/Th is ocean circulation. For p-coupled Pa/Th, it is coupled to ecosystem, therefore, is influenced by both ocean circulation and particle flux. For example, during HS1, both AMOC and productivity is suggested to be changed which will influence Pa/Th. Therefore, it is hard to detangle these two effects. Our model can help to solve this problem. For example, in our model, if we add freshwater forcing to North Atlantic, both productivity and AMOC changes will influence p-coupled Pa/Th. But in p-fixed Pa/Th is only influenced by AMOC change. Therefore, the effect of particle flux can be approximately estimated as p-couple minus p-fixed (line 86-93).

Table 2: Please add p-fixed or p-coupled to the scenarios respectively.

We add clarification as suggested (lin 888-891). As stated in Section 3 (line 207-209), both p-fixed and p-coupled are in CTRL, but only p-fix is available in Exp_1 and Exp_2 for computational efficiency. The p-fixed and p-coupled results in CTRL are identical (Line 235-244).

Table 3: Is there a reason for the iterating and non-iterating grey layers? Some references appear twice.

There is no particular reason for the iterating and non-iterating grey layers. The left column is references for water column activity and the right column is for Holocene core top Pa/Th. Some references have both column activity and Pa/Th, therefore appear twice.

Line 216: I do not agree the parameter set used by (Siddall et al., 2005) is a reasonable choice, only because "[…] the control experiment in Siddall et al., (2005) is able to simulate major features of 231Pa and 230Th distributions […]". Choosing the parameter

set more carefully and based on more recent approaches may help yielding more realistic simulations. (Rempfer, Stocker, Joos, Lippold, & Jaccard, 2017) listed different experimental studies suggesting a more balanced choice on K values. With the upper limit K value used for opal by (Siddall et al., 2005) the particle effect are inevitably overestimated.

In recent studies by Rempfer et al., 2017, they include bottom scavenging and boundary scavenging. In their study, they fix the fractionation factor (f, in their study, table A1 in their supplementary information, fractionation of ^{231}Pa and ^{230}Th by a certain particle type) and use scavenging efficiency as a tuning parameter (σ_0, in their study), keeping the fractionation factor the same. As they have pointed out, information about fractionation by different particles are still very limited (Chase et al., 2002; Scholten et al., 2005; Walter et al., 1997). The fractionation factor for opal used in our study is 0.3, while it is 1 in Rempfer et al., 2017. Observations suggests 0.2 from Luo & Ku, 2004, 0.3 from Chase et al., 2002 and 2.8 from Geibert & Usbeck, 2004. The fractionation factor for CaCO3 in our study is 40, while it is 10 in Rempfer et al., 2017. Observations suggests 3.8 from Roberts et al., 2009, 10 from Luo & Ku, 2004, 2.3-37 from Geibert & Usbeck, 2004 and 42 from Chase et al., 2002. Fractionation factor suggested by observations varies and our choice is in the range of observations. We agree that more sensitivity experiments will definitely help to improve the model performance. Our study is the first step trying to implementing ^{231}Pa and ^{230}Th into CESM. The parameters can be improved in the future with more observations available (line 489-492).

Line 230 and Fig. 9: a freshwater input of 1 Sv for 1.2 ka is way too high in order to simulate any past fresh-water flux (Carlson & Clark, 2012). If the authors want to show that AMOC and 231Pa/230Th are a function of fresh-water flux then their study is presented approx. 20 years too late. But if they want to improve our knowledge on the reaction of 231Pa/230Th on realistic fresh-water fluxes of the past, they should lower the fresh-water input. I think the authors miss an opportunity here.

Thanks for pointing this out. We agree 1 Sv is too high for realistic fresh water forcing. However, in our idealized ocean alone experiment under present day climate forcing, fresh water has to be this large to shut down AMOC. We have run several different experiments, with fresh water forcing increasing from 0 to 1 Sv (Table below). If fresh water is 0.1 Sv, which is the order of realistic fresh water flux during Heinrich Event Stadial 1 (HS1), the AMOC is reduced only a little compared with control experiment. However, using the same model, under realistic forcing, this model is able to simulate the transient AMOC responses from 22ka to 13ka (Zhang et al., 2017). Therefore, AMOC response may depend on the initial climatology or depend on the location of fresh water forcing, which is out of the scope of this study. In our study, our experiments are highly idealized and we want to test how ^{231}Pa/^{230}Th responds to AMOC change. To shut down AMOC, we have to use this unrealistically large fresh water flux.

FW (50-70N)	**0**	**0.1**	**0.3**	**0.5**	**0.7**	**1.0**
AMOC	15.6	13.4	8.7	4.9	3.4	2.0

They also miss an opportunity by not-implementing bottom-scavenging. There are new GEOTRACES data out, which suggest non-negligible effects from nepheloid layers on 231Pa/230Th. I would expect that (at least for p-fixed) this would be very laborious.

We agree nepheloid layers are important. Rempfer et al., 2017 came out after we have prepared our study. Their results suggest that the relationship between $^{231}Pa/^{230}Th$ and AMOC is not affected by boundary scavenging or bottom scavenging (pointed out in line 200-204). Therefore, since we are focusing on sediment $^{231}Pa/^{230}Th$ instead of water column activity, our results will not be influenced too much by including nepheloid layer. However, nepheloid layer must be included in future works. We have included this in line 487-489.

Lien 242: I don't understand this sentence at all. There is a reference to statistical values in Fig. 4a which are not there.

Sorry there is no longer values in Fig.4 after modification in our last version. We have deleted this reference in the text (line 240).

Figure 5: I cannot follow the statistics provided here. The yellow points in 5a hardly lead to a slope close to 1.

The purple line in Fig.5 is the least squared liner regression. For shallow layers, model results are much smaller than observation (red, blue dots). For deep layers, model results are much larger than observation (yellow dots). The least squared method of regression gives the result of the purple line and the slope is 1.02.

Line 259: I think I cannot accept that the dissolved fractions are simulated so utterly bad, simply "[…] because boundary scavenging and sediment resuspensions are not included in our model […]". I suggest first that the authors re-examine the observational data. Which of the outliers (e.g. Fig. 5c) are reliable values with reasonable errors? Because what can we learn from a parameter set and model which is not able to reconstruct the magnitude of the particulate fraction. If this was already a problem in the studies by (Dutay, Lacan, Roy-Barman, & Bopp, 2009) and (Siddall et al., 2005), why not recalibrate the model? How did (Rempfer et al., 2017) cope with this problem?

In Fig 2 and 3, we show water column dissolved ^{231}Pa and ^{230}Th activity and the particulate $[^{231}Pa/^{230}Th]_p$ along two GEOTRACES transects. What each figure is about is listed at the top left of each figure. In both transects, the dissolved ^{231}Pa and ^{230}Th activity is too large in the abyssal compared with observations. That why we state that "Our model is unable to simulate the realistic dissolved 231Pa and 230Th activities in abyssal" in line 257-258. In Rempfer et al., 2017, they also show dissolved ^{231}Pa and ^{230}Th activity and the particulate $[^{231}Pa/^{230}Th]_p$ along the same two GEOTRACES transects. They show results in Re3d (without boundary scavenging and nepheloid layer), Rd3d_Bd (with boundary scavenging but with nepheloid layer), and Rd3d_BtBd (with boundary scavenging and nepheloid layer). There results shows that water column dissolved ^{231}Pa and ^{230}Th activity is very large in abyssal if there is no boundary scavenging and nepheloid layer (Re3d), which is similar to our results. But in Rd3d_BtBd, the water column dissolved ^{231}Pa and ^{230}Th activity is in the right magnitude compared with observation. This suggests that boundary scavenging and nepheloid layer are important

for simulating dissolved ^{231}Pa and ^{230}Th activity in abyssal. That's why we state that "With boundary scavenging and sediment resuspensions added, dissolved ^{231}Pa and ^{230}Th activities in the abyssal should be reduced" in line 259-261.

Line 281: "The sediment 231Pa/230Th in CTRL is overall consistent with observations [...]". Wouldn't it be interesting to go into more detail here? Where are they consistent? Which basin, which water depth? Is margin distance an issue? By carving out which region is worse represented than others a lot could be learned about and from the model. E.g. Southern Ocean: because opal fluxes are so high 231Pa/230Th can vary a lot (much more than in the Atlantic). Simulating correct absolute values is almost impossible because opal flux varies on very small spatial scales, which cannot be captured by any model. Thus, the quality of the model run assessed by observations from this area will inevitably lead to bad agreement.

We appreciate this suggestion. In this part, we are focusing on large scale sediment ^{231}Pa/^{230}Th distribution, which our model is able to capture as discussed in line 281-296. We did not go into details about sediment ^{231}Pa/^{230}Th distribution because it is not the focus of this study. But details of model sediment ^{231}Pa/^{230}Th performance can be useful, for example, to improve model biogeochemical module, and therefore worth further study.

Line296: Where is the statement given here shown/demonstrated? Figure?

In Fig 1c, there is an opal maximum at about 40°N in the Atlantic. In this region, sediment ^{231}Pa/^{230}Th is also larger than surroundings (Fig. 4). We add this in line 296.

Line 303, Fig.6: I cannot follow the argumentation here. It would be necessary to increase the scale on Fig. 6and b in order to better resolve the high values. At the moment any variations are hidden within the red colour. The finding, that K influences dissolved fractions but not particulate fractions needs much more explanation. The simplification with reference to Eq. 3 and 7 does not help much.

Thanks for the suggestion. We have changed the color scale for Fig. 6 a and b. The overall structures of dissolved ^{231}Pa and ^{230}Th activity are similar in two sensitivity experiments, but the magnitude is much larger in Exp_1 (smaller K) than Exp_2 (larger K).

We have re-written this part (line 303-332). We first derive the particulate and dissolved isotope activity under the assumption that there is no isotope decay and no ocean transport (Eq. 7 and 8). This can help us understand the difference between Exp_1 and Exp_2. For dissolved isotope activity, Eq. 8 suggests that increased K will lead to decreased dissolved isotope activity. For particulate isotope activity, Eq. 7 suggests that particulate isotope activity is independent of K. Therefore, particulate isotope activity in Exp_1 and Exp_2 does not change too much, especially compared with the changes in dissolved isotope activity.

Table 2: More realistic values for EXP1 and 2 would be appreciated in order to derive helpful insights from the model runs.

In (Siddall et al., 2005), they show model sensitivity with K one order of magnitude larger or smaller than the CTRL. Our experiments are similar to theirs. We want to show that how water column activity and sediment $^{231}Pa/^{230}Th$ change with K and also the K used in the control experiment is of the right order of magnitude. We agree that more experiments with K changes slightly around control will be helpful. This will act as a parameter tuning process and worth the effort in future studies. We have added this part in line 489-492.

Line 329: This statement should be proved statistically (like Fig. 5).

Thanks for this suggestion. We have included the RMSE for different experiments in line 339-340. The parameters in CTRL produce the minimum RMSE comparing with Exp_1 and Exp_2.

Line 360: In the following paragraph the effects of opal on 231Pa/230Th is discussed. However, the model generates opal fluxes not in agreement with reality. In the response to the reviewer the authors claim that the large scale global opal production is reflected well in the model (e.g. high in SO). I agree. They also claim that the question, why the models produces a "fake-bloom" of opal production in the Western North Atlantic, is beyond the scope of this study. I may accept this (but then one may questioning the validity of the model approach), however in this case the paragraph following line 360 needs to be written more carefully and with a clear statement, that opal is not well represented on smaller spatial scales. Same with line 409.

Thanks for this suggestion. It is hard to reproduce the productivity everywhere, especially on small scales. The productivity pattern produced by the biogeochemical module is consistent with observations over most regions. Model is never perfect. As long as it can help us understand something, it is useful. The opal bloom in the northwest Atlantic produced by the biogeochemical module in the CESM is not in the observation. But at least the pattern of Pa/Th response to the fresh water hosing is self-consistent with the productivity pattern in our model and can give some insights of interpreting sediment Pa/Th. We have added this part in line 377-380.

Line 419: Of course studies on AMOC reconstructions need to cross check opal fluxes, but this sentence spreads a way too negative message when based on unrealistic opal fluxes and hence I do not agree. Please rephrase.

Thanks for this suggestion. We have changed in line 438-439.

Fig 9: the difference between coupled and fixed are partly so big, that I wonder how both methods did agree so well before. Differences in the range of Δ231Pa/230Th>0.1 (e.g. 9d) are not increasing my confidence in the model. Observations are much more constrained. Again I plead for applying realistic model parameters only. Further, I could not find information on water depth and longitude of the values shown in Fig. 9 diagrams, which are essential for the interpretation.

The big difference between coupled and fixed in HOSING is the point we want to make: the particle fields matters. At time 0, when there is no freshwater forcing (CTRL

experiment), the fixed and coupled are the same. This is what shown in Fig. 4 and discussed in line 235-244: in CTRL, p-fixed and p-coupled results are identical, which is because the particle fields are essentially the same (control experiment, no extra forcing). However, when freshwater is added, both AMOC and particle field produced by biogeochemical module (Fig.8) change. E.g. Fig.9d, for p-fixed curve (green), the particle field is held the same. The increase of Pa/Th is caused by the reduce of AMOC. For p-coupled curve (red), AMOC will lead to an increase in Pa/Th (similar to the green curve), but particle change effect at this site will lead to a decrease in Pa/Th. Therefore, p-coupled Pa/Th at equilibrium (red) is much smaller than p-fixed Pa/Th (green). The difference between p-fixed and p-coupled is caused by the change of particle fields (Fig. 8). In reconstructions, it is hard to know how much Pa/Th change is caused by AMOC and how much is by particle. But in our model, by comparing p-fixed with p-coupled results, we can detangle the AMOC effect and particle effect. This is the point we have emphasized in several places (e.g. line 89-93, line 411-416 and line 417-439)

Fig.9 c-f are four sites picked in the North Atlantic to representing different mechanisms. The depth of each site is decided by the model topography (bottom cell at that location). Locations for Fig.9 c-f are picked for different reasons: (c) is a location in high latitude North Atlantic where opal production increases after applying fresh water forcing over 50°N-70°N (Fig. 8f); (d) is a location where opal production is the maximum in our model; (e) and (f) are locations near Bermuda Rise (McManus et al., 2004). These four locations behave differently in HOSING as discussed in section 4.3 (line 411-439)

Line 424: Why is there a decrease of 231Pa/230Th above 2 km only? To my understanding and as stated in line 442 the decrease affects all of the NADW seized water depths.

The pattern in Fig. 12 is also produced in Rempfer et al., 2017 (their Fig. 8). Vertical decrease of Pa_p/Th_p is suggested to be caused by the lateral transport by AMOC (line 277-280). Northward transport in the upper limb of AMOC will lead to ^{231}Pa import while southward transport in the lower limb of AMOC will lead to ^{231}Pa export. Therefore, we see a vertical decrease of ^{231}Pa/^{230}Th (Fig. 12c). If there is no more ocean transport by AMOC, then there is no more ^{231}Pa import for upper layer and ^{231}Pa/^{230}Th shows a decrease, and vice versa for deep layer. This is explained in detail in line 451-463.

Line 460: Yes, the parameters are somewhere in the range of the right magnitude, but not more. It would be great if this study would help to represent 231Pa/230Th in a realistic model, not only somewhere in the range of a factor of 25.

We have change this to “right order of magnitude” (line 341).

Fig10b: site locations are not visible.

We have enlarged the site location in this figure.

Fig12c: Please explain the change of direction of 231Pa/230Th with depth at about 4000m for ON

The increase of Pa/Th at about 4,000m for AMOC_on case is probably caused by AABW transport. AABW from the Southern Ocean transport ^{231}Pa enriched water northward, which results in the increase of Pa/Th. This is similar to the argument by (Thomas et al., 2006) (line 66-72).

Reference:

Chase, Z., Anderson, R. F., Fleisher, M. Q., & Kubik, P. W. (2002). The influence of particle composition and particle flux on scavenging of Th , Pa and Be in the ocean. *Earth and Planetary Science Letters*, *204*(1–2), 215–229. https://doi.org/10.1016/S0012-821X(02)00984-6

Geibert, W., & Usbeck, R. (2004). Adsorption of thorium and protactinium onto different particle types: Experimental findings. *Geochimica et Cosmochimica Acta*, *68*(7), 1489–1501. https://doi.org/10.1016/j.gca.2003.10.011

Luo, S., & Ku, T. L. (2004). On the importance of opal, carbonate, and lithogenic clays in scavenging and fractionating 230Th, 231Pa and 10Be in the ocean. *Earth and Planetary Science Letters*, *220*(1–2), 201–211. https://doi.org/10.1016/S0012-821X(04)00027-5

McManus, J., Francois, R., & Gherardi, J. (2004). Collapse and rapid resumption of Atlantic meridional circulation linked to deglacial climate changes. *Nature*, *428*(6985), 834–837.

Rempfer, J., Stocker, T. F., Joos, F., Lippold, J., & Jaccard, S. L. (2017). New insights into cycling of 231 Pa and 230 Th in the Atlantic Ocean. *Earth and Planetary Science Letters*, *468*, 27–37. https://doi.org/10.1016/j.epsl.2017.03.027

Roberts, K. A., Xu, C., Hung, C. C., Conte, M. H., & Santschi, P. H. (2009). Scavenging and fractionation of thorium vs. protactinium in the ocean, as determined from particle-water partitioning experiments with sediment trap material from the Gulf of Mexico and Sargasso Sea. *Earth and Planetary Science Letters*, *286*(1–2), 131–138. https://doi.org/10.1016/j.epsl.2009.06.029

Scholten, J. C., Fietzke, J., Mangini, A., Stoffers, P., Rixen, T., Gaye-Haake, B., … Ittekkot, V. (2005). Radionuclide fluxes in the Arabian Sea: The role of particle composition. *Earth and Planetary Science Letters*, *230*(3–4), 319–337. https://doi.org/10.1016/j.epsl.2004.11.003

Siddall, M., Henderson, G. M., Edwards, N. R., Frank, M., Müller, S. a., Stocker, T. F., & Joos, F. (2005). 231Pa/230Th fractionation by ocean transport, biogenic particle flux and particle type. *Earth and Planetary Science Letters*, *237*(1–2), 135–155. https://doi.org/10.1016/j.epsl.2005.05.031

Thomas, A. L., Henderson, G. M., & Robinson, L. F. (2006). Interpretation of the 231Pa/230Th paleocirculation proxy: New water-column measurements from the southwest Indian Ocean. *Earth and Planetary Science Letters*, *241*(3–4), 493–504. https://doi.org/10.1016/j.epsl.2005.11.031

Walter, H. J., Rutgers van der Loeff, M. M., & Hoeltzen, H. (1997). Enhanced

scavenging of 231Pa relative to 230Th in the South Atlantic south of the Polar Front: Implications for the use of the 231Pa/230Th ratio as a paleoproductivity proxy. *Earth and Planetary Science Letters*, *149*(1), 85–100. https://doi.org/10.1016/S0012-821X(97)00068-X

Zhang, J., Liu, Z., Brady, E. C., Jahn, A., Oppo, D. W., Clark, P. U., … Lindsay, K. (2017). Asynchronous warming and oxygen isotope evolution of deep Atlantic water masses during the last deglaication. *Proceedings of the National Academy of Sciences*, *In revisio*, 2–7. https://doi.org/10.1073/pnas.1704512114

^{231}Pa and ^{230}Th in the ocean model of the Community Earth System Model (CESM1.3)

Sifan Gu[1], Zhengyu Liu[1,2]

[1]Department of Atmospheric and Oceanic Sciences and Center for Climate Research, University of Wisconsin-Madison, Madison, WI, USA

2. Now, affiliated with: Atmospheric Science Program, Department of Geography, Ohio State University, Columbus, OH, USA

Correspondence to: Sifan Gu (sgu28@wisc.edu)

Abstract

Sediment ^{231}Pa/^{230}Th activity ratio is emerging as an important proxy for deep ocean circulation in the past. In order to allow for a direct model-data comparison and to improve our understanding of sediment ^{231}Pa/^{230}Th activity ratio, we implement ^{231}Pa and ^{230}Th in the ocean component of the Community Earth System Model (CESM). In addition to the fully coupled implementation of the scavenging behavior of ^{231}Pa and ^{230}Th with the active marine ecosystem module (p-coupled), another form of ^{231}Pa and ^{230}Th have also been implemented with prescribed particle flux fields of the present climate (p-fixed). The comparison of the two forms of ^{231}Pa and ^{230}Th helps to isolate the influence of the particle fluxes from that of ocean circulation. Under present day climate forcing, our model is able to simulate water column ^{231}Pa and ^{230}Th activity and sediment ^{231}Pa/^{230}Th activity ratio in good agreement with available observations. In addition, the p-coupled and p-fixed sediment ^{231}Pa/^{230}Th activity ratios behave similarly over large areas of low productivity on long timescale to freshwater forcing, but can differ substantially in some regions of high productivity and on short timescale, indicating the importance of biological productivity in addition to ocean transport. Therefore, our model provides a potentially powerful tool to help our interpretation of sediment ^{231}Pa/^{230}Th reconstructions and to improve our understanding of past ocean circulation and climate changes.

Formatted: Justified, Line spacing: 1.5 lines

Deleted: physical circulation

Deleted: ... [1]

1. Introduction

Sediment $^{231}Pa/^{230}Th$ activity ratio has been used as a proxy for ocean circulation in the past (e.g. Yu et al. 1996; McManus et al. 2004; Gherardi et al. 2009). ^{231}Pa (32.5 ka half-life) and ^{230}Th (75.2 ka half-life) are produced at a constant rate approximately uniformly in the ocean by the α decay of ^{235}U and ^{234}U, respectively, with a production activity ratio of 0.093 (Henderson and Anderson, 2003). Water column ^{231}Pa and ^{230}Th are subject to particle scavenging and transport to sediments (Bacon and Anderson, 1982; Nozaki et al., 1987). Different scavenging efficiency results in different ocean residence time: ^{231}Pa has a residence time of approximately 111 years and ^{230}Th has a residence time of approximately 26 years (Yu et al., 1996). Longer residence time of ^{231}Pa than ^{230}Th makes ^{231}Pa more subject to ocean transport and therefore in the modern ocean about 45% of ^{231}Pa produced in the Atlantic is transported to the Southern Ocean (Yu et al., 1996), resulting a lower than 0.093 sediment $^{231}Pa/^{230}Th$ activity ratio in the North Atlantic and higher than 0.093 sediment $^{231}Pa/^{230}Th$ activity ratio in the Southern Ocean.

The application of the principle above to interpret sediment $^{231}Pa/^{230}Th$ as the strength of Atlantic meridional overturning circulation (AMOC), however, can be complicated by other factors, leading to uncertainties in using $^{231}Pa/^{230}Th$ as a proxy for past circulation (Keigwin and Boyle, 2008; Lippold et al., 2009; Scholten et al., 2008). In addition to the ocean transport, sediment $^{231}Pa/^{230}Th$ is also influenced by particle flux and composition (Chase et al., 2002; Geibert and Usbeck, 2004; Scholten et al., 2008; Siddall et al., 2007; Walter et al., 1997). The region of a higher particle flux tends to have a higher $^{231}Pa/^{230}Th$ (Kumar et al., 1993; Yong Lao et al., 1992), which is referred to as the "particle flux effect" (Siddall et al., 2005). Regional high particle flux in the water column will favor the removal of isotopes into the sediment, which leads to more isotopes transported into this region due to the down-gradient diffusive flux and subsequently more removal of isotopes into the sediment. Since ^{231}Pa has a longer residence time, this effect is more prominent on ^{231}Pa than on ^{230}Th and therefore sediment $^{231}Pa/^{230}Th$ will be higher in high productivity regions. Also, opal is able to scavenge ^{231}Pa much more effectively than ^{230}Th, leading to higher $^{231}Pa/^{230}Th$ in high opal flux regions such as the Southern

Deleted: to reconstruct

Deleted: M

Deleted: O

Deleted: C

Deleted: paleo

Deleted: H

Deleted: in a region

Ocean (Chase et al., 2002). Moreover, sediment $^{231}Pa/^{230}Th$ is suggested to record circulation change only within 1,000 m above the sediment, instead of the whole water column, complicating the interpretation of sediment $^{231}Pa/^{230}Th$ reconstructions (Thomas et al., 2006). For example, sediment $^{231}Pa/^{230}Th$ approaching 0.093 during Heinrich Stadial event 1(HS1) from the subtropical North Atlantic is interpreted as the collapse of AMOC (McManus et al., 2004). If sediment $^{231}Pa/^{230}Th$ only records deepest water mass, it is possible that during HS1, AMOC shoals, as opposed to a fully collapse, yet an increase of deep water imported from the Southern Ocean featuring high $^{231}Pa/^{230}Th$ can increase the sediment $^{231}Pa/^{230}Th$ approaching the production ratio (0.093) (Thomas et al., 2006). Therefore, it is important to incorporate ^{231}Pa and ^{230}Th into climate models for a direct model-data comparison and to promote a thorough understanding of sediment $^{231}Pa/^{230}Th$ as well as past ocean circulation.

^{231}Pa and ^{230}Th have been simulated in previous modeling studies (Dutay et al., 2009; Luo et al., 2010; Marchal et al., 2000; Rempfer et al., 2017; Siddall et al., 2005). Marchal et al., (2000) simulates ^{231}Pa and ^{230}Th in a zonally averaged circulation model, using the reversible scavenging model of Bacon and Anderson, (1982). One step further, Siddall et al. (2005) extends Marchal et al., (2000) by including particle dissolution with prescribed particle export production in a 3-D circulation model. Rempfer et al., (2017) further couples ^{231}Pa and ^{230}Th with active biogeochemical model and includes boundary scavenging and sediment resuspensions to improve model performance in simulating water column ^{231}Pa and ^{230}Th activity. Here we follow previous studies to implement ^{231}Pa and ^{230}Th into the Community Earth System Model (CESM). Our ^{231}Pa and ^{230}Th are coupled with active marine ecosystem model ("p-coupled") and p-coupled $^{231}Pa/^{230}Th$ is influenced by both ocean circulation change and particle flux change. To help to understand the influence of the particle flux, we have also implemented a "p-fixed" version of ^{231}Pa and ^{230}Th, for which the particle fluxes are fixed at prescribed values. Therefore, p-fixed $^{231}Pa/^{230}Th$ is only influenced by ocean circulation change. By comparing the p-fixed $^{231}Pa/^{230}Th$ with the p-coupled $^{231}Pa/^{230}Th$, we will be able to separate the effect of circulation change from particle flux change. In

Deleted: the Atlantic meridional Overturning Circulation (

Deleted:)

Formatted: Not Superscript/ Subscript

Deleted: All these suggest the

Deleted: ce

Deleted: of

Deleted: incorporating

Deleted: for

Deleted: concentration

Deleted: model

Deleted:

Deleted: therefore can be used to study the impact of ecosystem change on ^{231}Pa and ^{230}Th directly

Deleted: .

Deleted: By

Deleted: and

Deleted: and

Deleted: field

addition, the p-fixed ^{231}Pa and ^{230}Th can be run without the marine ecosystem module, reducing computational cost by a factor of 3 in the ocean-alone model simulation, making it a computationally efficient tracer for sensitivity studies.

This paper describes the details of ^{231}Pa and ^{230}Th in CESM and serves as a reference for future studies using this tracer module. In section 2, we describe the model and the implementation of ^{231}Pa and ^{230}Th. In sections 3, we describe the experimental design. We will finally compare simulated ^{231}Pa and ^{230}Th fields with observations, show model sensitivities on model parameter and also sediment ^{231}Pa/^{230}Th ratio response to freshwater forcing in Section 4.

2. Model Description

2.1 Physical Ocean Model

We implement ^{231}Pa and ^{230}Th in the ocean model (Parallel Ocean Program version 2, POP2) (Danabasoglu et al., 2012) of CESM (Hurrell et al., 2013). CESM is a state-of-the-art coupled climate model and studies describing model components and analyzing results can be found in a special collection in Journal of Climate (http://journals.ametsoc.org/topic/ccsm4-cesm1). We run the ocean-alone model, which is coupled to data atmosphere, land, ice and river runoff under the normal year forcing of CORE-II data (Large and Yeager, 2008), using the low-resolution version of POP2 with a nominal 3° horizontal resolution and 60 vertical layers.

2.2 Biogeochemical component (BGC)

CESM has incorporated a marine ecosystem module that simulates biological variables (Moore et al., 2013). The marine ecosystem module has been validated against present day observations extensively (e.g. Doney et al., 2009; Long et al., 2013; Moore et al., 2002, 2004; Moore and Braucher, 2008). The implementation of ^{231}Pa and ^{230}Th requires particle fields: $CaCO_3$, opal and particulate organic carbon (POC). These particle fields can be obtained through the ecosystem driver from the ecosystem module (Jahn et al., 2015). The ecosystem module simulates the particle fluxes in reasonable agreement with the present-day observations. The pattern and magnitude of the annual mean particle fluxes ($CaCO_3$, opal, POC) leaving the

Deleted: and therefore

Deleted: the

Deleted: from

Deleted: present day

euphotic zone at 105m are similar to the satellite observations (Fig. 7.2.5 and 9.2.2 in Sarmiento and Gruber 2006) (Fig. 1 a~c): particle fluxes are higher in the high productivity regions such as high latitudes and equatorial Pacific; opal flux is high in the Southern Ocean. The remineralization scheme of particle is based on the ballast model of Armstrong et al., (2002). Detailed parameterizations for particle remineralization are documented in Moore et al., (2004) with temperature dependent remineralization length scales for POC and opal. We do not consider dust because it is suggested to be unimportant for ^{231}Pa and ^{230}Th fractionation (Chase et al., 2002; Siddall et al., 2005).

2.3 ^{231}Pa and ^{230}Th implementation

^{231}Pa and ^{230}Th are produced from the α decay of ^{235}U and ^{234}U uniformly everywhere at constant rate β^i (β^{Pa} = 2.33*10^{-3} dpm m^{-3} yr^{-1}, β^{Th} = 2.52*10^{-2} dpm m^{-3} yr^{-1}). ^{231}Pa and ^{230}Th are also subjective to radioactive decay with the decay constant of λ^i (λ^{Pa} = 2.13*10^{-5} yr^{-1}, λ^{Th} = 9.22*10^{-6} yr^{-1}).

Another important process contributes to ^{231}Pa and ^{230}Th activity is the reversible scavenging by sinking particles (Bacon and Anderson, 1982), which describes the adsorption of isotopes onto sinking particles and desorption after the dissolution of particles. This process transports ^{231}Pa and ^{230}Th downward and leads to a general increase of ^{231}Pa and ^{230}Th activity with depth. The reversible scavenging considers total isotope activity (A_t^i) as two categories (Eq. (1)): dissolved isotopes (A_d^i) and particulate isotopes (A_p^i) (superscript i refers to ^{231}Pa and ^{230}Th) and A_p^i is the sum of the isotopes associated with different particle types ($A_{j,p}^i$) (subscript j refers to different particle types: $CaCO_3$, opal and POC):

$$A_t^i = A_d^i + A_p^i = A_d^i + \sum_j A_{j,p}^i \quad (1)$$

Dissolved and particulate isotopes are assumed to be in equilibrium, which is a reasonable assumption in the open ocean (Bacon and Anderson, 1982; Henderson et

al., 1999; Moore and Hunter, 1985). The ratio between the particulate isotope activity and the dissolved isotope activity is set by a partition coefficient, K (Eq. (2)):

$$K_j^i = \frac{A_{j,p}^i}{A_d^i \cdot R_j} \quad (2)$$

, where R_j is the ratio of particle concentration (C_j) to the density of seawater (1024.5 kg m^{-3}). Subscript j refers to different particle types ($CaCO_3$, opal and POC). Values of partition coefficient K used in our control simulation follows Chase et al., 2002 and Siddall et al., 2005 (Table 2).

Particulate isotopes (A_p^i) will be transported by sinking particles, which is described by $w_S \frac{\partial A_p^i}{\partial z}$ (Eq. (3)), where w_s is the sinking velocity. We don't differentiate between slow sinking small particles and rapid sinking large particles as in Dutay et al., (2009) and consider all particles as slowly sinking small particles with sinking velocity of w_s =1000 m yr^{-1} (Arsouze et al., 2009; Dutay et al., 2009; Kriest, 2002), which is similar to Rempfer et al., (2017) and Siddall et al., (2005). Any particulate isotopes (A_p^i) at the ocean bottom layer are removed from the ocean as sediment, which is the sink for the isotope budget. Detailed vertical differentiation scheme to calculate this term in the model is provided in the supplementary material. The reversible scavenging scheme applied here is the same as the neodymium implementation in POP2 (Gu et al., 2017).

Therefore, the conservation equation for ^{231}Pa and ^{230}Th activity can be written as

$$\frac{\partial A_t^i}{\partial t} = \beta^i - \lambda^i A_t^i - w_s \frac{\partial A_p^i}{\partial z} + Transport \quad (3),$$

where the total isotope activity is controlled by decay from U (first term), radioactive decay (second term), reversible scavenging (third term) and physical

Deleted: as in

Deleted:

Deleted: (Gu et al., 2017)

Moved down [3]: Particle fields used in the reversible scavenging can be either prescribed or simultaneously generated from the marine ecosystem module. Therefore, two forms of ^{231}Pa and ^{230}Th are implemented in POP2: "p-fixed" and "p-coupled". P-fixed ^{231}Pa and ^{230}Th use particle fluxes prescribed as annual mean particle fluxes generated from the marine ecosystem module under present day climate forcing (Fig.1). P-coupled ^{231}Pa and ^{230}Th use particle fluxes computed simultaneously from the marine ecosystem module. P-fixed and p-coupled ^{231}Pa and ^{230}Th can be turned on at the case build time and the p-coupled ^{231}Pa and ^{230}Th requires the ecosystem module to be turned on at the same time.

transport by the ocean model (fourth term, including advection, convection and diffusion). A_p^i can be calculated by combining Eq. (1) and Eq. (2):

$$A_t^i = A_d^i + A_d^i \cdot (K_{POC}^i \cdot R_{POC} + K_{CaCO_3}^i \cdot R_{CaCO_3} + K_{opal}^i \cdot R_{opal})$$
$$= A_d^i \cdot (1 + K_{POC}^i \cdot R_{POC} + K_{CaCO_3}^i \cdot R_{CaCO_3} + K_{opal}^i \cdot R_{opal}), \quad (4)$$

which leads to

$$A_d^i = \frac{A_t^i}{1 + K_{POC}^i \cdot R_{POC} + K_{CaCO_3}^i \cdot R_{CaCO_3} + K_{opal}^i \cdot R_{opal}}, \quad (5)$$

put this back to Eq. (1), we get

$$A_p^i = A_t^i \cdot (1 - \frac{1}{1 + K_{POC}^i \cdot R_{POC} + K_{CaCO_3}^i \cdot R_{CaCO_3} + K_{opal}^i \cdot R_{opal}}) \quad (6)$$

Particle fields used in the reversible scavenging can be either prescribed or simultaneously generated from the marine ecosystem module. Therefore, two forms of ^{231}Pa and ^{230}Th are implemented in POP2: "p-fixed" and "p-coupled". P-fixed ^{231}Pa and ^{230}Th use particle fluxes prescribed as annual mean particle fluxes generated from the marine ecosystem module under present day climate forcing (Fig.1). P-coupled ^{231}Pa and ^{230}Th use particle fluxes computed simultaneously from the marine ecosystem module. P-fixed and p-coupled ^{231}Pa and ^{230}Th can be turned on at the case build time and the p-coupled ^{231}Pa and ^{230}Th requires the ecosystem module to be turned on at the same time.

Moved (insertion) [3]

Comparing with previous studies of modeling ^{231}Pa and ^{230}Th, our p-fixed version is the same as Siddall et al., (2002), except that different prescribed particle fluxes are used. The p-coupled version allows coupling to biogeochemical module, which is similar to Rempfer et al., (2017), but we do not include boundary scavenging and sediment resuspensions as in Rempfer et al., (2017) because boundary scavenging and sediment resuspensions are suggested to be unimportant to influence the relationship between $^{231}Pa_p/^{230}Th_p$ and AMOC strength (Rempfer et al., 2017).

Formatted: Indent: First line: 0.5"

Deleted: in

3. Experiments

We run a control experiment (CTRL) and two experiments with different partition coefficients to show model sensitivity. We have both p-fixed and p-coupled ^{231}Pa and ^{230}Th in CTRL, but only p-fixed ^{231}Pa and ^{230}Th in sensitivity experiments. Equilibrium partition coefficients for ^{231}Pa and ^{230}Th vary among different particle types and the magnitude of the partition coefficients for different particle types remains uncertain (Chase et al., 2002; Chase and Robert F, 2004; Luo and Ku, 1999). Since the control experiment in Siddall et al., (2005) is able to simulate major features of ^{231}Pa and ^{230}Th distributions, we use the partition coefficients from the control experiment in Siddall et al., (2005) in our CTRL (Table 2). Two sensitivity experiments are performed with decreased (EXP_1) and increased (EXP_2) partition coefficients by a factor of 5 (Table 2).

All the experiments are ocean-alone experiments with the normal year forcing by CORE-II data (Large and Yeager, 2008). The ^{231}Pa and ^{230}Th activities are initiated from 0 in CTRL and are integrated for 2,000 model years until equilibrium is reached. EXP_1 and EXP_2 are initiated from 1,400 model year in CTRL and are integrated for another 800 model years to reach equilibrium.

Since sediment ^{231}Pa/^{230}Th in North Atlantic has been used to reflect the strength of AMOC, to test how sediment ^{231}Pa/^{230}Th in our model responds to the change of AMOC and the change of particle fluxes, we carried out a fresh water perturbation experiment (HOSING) with both p-fixed and p-coupled ^{231}Pa and ^{230}Th. Starting from 2,000 model year of CTRL, a freshwater flux of 1 Sv is imposed over the North Atlantic region of 50°N~70°N and the experiment is integrated for 1400 model years until both p-fixed and p-coupled sediment ^{231}Pa/^{230}Th ratio have reached quasi-equilibrium. The partition coefficients used in HOSING are the same as in CTRL.

4. Results

4.1 Control Experiment

P-fixed and p-coupled version of ^{231}Pa and ^{230}Th in CTRL show identical results (Fig. 2-4). P-fixed and p-coupled dissolved and particulate ^{231}Pa and ^{230}Th in

Deleted: to partition coefficient

CTRL are highly correlated with each other with correlations greater than 0.995 and regression coefficients are all near 1.0 (R^2>0.995). The correlation coefficient between p-fixed and p-coupled sediment $^{231}Pa/^{230}Th$ activity ratios in CTRL is 0.99 and the regression coefficient is 0.9 (R^2=0.98). This is expected because the particle fields used in p-fixed version are prescribed as the climatology of the particle fields used in the p-coupled version. Therefore, under the same climate forcing, p-fixed and p-coupled version of ^{231}Pa and ^{230}Th should be very similar. For the discussion of results in CTRL below, we only discuss the p-fixed ^{231}Pa and ^{230}Th.

The residence time of both ^{231}Pa and ^{230}Th in CTRL are comparable with observations. The residence time is calculated as the ratio of global average total isotope activity and the radioactive ingrowth of the isotope. Residence time in CTRL is 118 yr for ^{231}Pa and 33 yr for ^{230}Th (Table 2), which are of the same magnitude as 111 yr for ^{231}Pa and 26 yr for ^{230}Th in observation (Yu et al., 1996).

CTRL can simulate the general features of dissolved water column ^{231}Pa and ^{230}Th activities. Dissolved ^{231}Pa and ^{230}Th activities increase with depth in CTRL, as shown in two GEOTRACES transects (Deng et al., 2014; Hayes et al., 2015) in the Atlantic (Fig. 2 and 3). The dissolved ^{231}Pa and ^{230}Th activities in CTRL are also at the same order of magnitude as in observations in the most of the ocean, except that simulated values are larger than observations in the abyssal, which is also the case in Siddall et al., (2005) and Rempfer et al., (2017) (their Fig. 2 and 3, experiment Re3d). Our model is unable to simulate the realistic dissolved ^{231}Pa and ^{230}Th activities in abyssal because boundary scavenging and sediment resuspensions are not included in our model. With boundary scavenging and sediment resuspensions added, dissolved ^{231}Pa and ^{230}Th activities in the abyssal should be greatly reduced (Rempfer et al., 2017).

A more quantitative model-data comparison is shown in Fig. 5. The linear regression coefficient between model results and observations (references of observations are listed in Table 3), an indication of model ability to simulate ^{231}Pa and ^{230}Th activity (Dutay et al., 2009), is near 1.0 for dissolved ^{231}Pa and ^{230}Th (1.02 for $[^{231}Pa]_d$ and 1.14 for $[^{230}Th]_d$), suggesting that CTRL can simulate the dissolved ^{231}Pa and ^{230}Th in good agreement with observations. However, the simulation of

Deleted: larger

Deleted: (Fig. 4a).

the particulate activity is not as good as the dissolved activity. Particulate activity is overall larger than observation in the surface ocean and smaller than observation in the deep ocean for both particulate ^{231}Pa and ^{230}Th. The regression coefficient for particulate ^{231}Pa and ^{230}Th is 0.02 for $[^{231}Pa]_p$ and 0.05 for $[^{230}Th]_p$. The poor performance in simulating water column particulate ^{231}Pa and ^{230}Th activities is also in previous modeling studies (Dutay et al., 2009; Siddall et al., 2005), because of similar modelling scheme are applied. However, the simulated $^{231}Pa_p/^{230}Th_p$ is in reasonable agreement with observations. The $^{231}Pa_p/^{230}Th_p$ along two GEOTRACES transects (Fig. 2 and 3) show the similar pattern and magnitude as in Rempfer et al., (2017), consistent with observations. Decrease of $^{231}Pa_p/^{230}Th_p$ with depth is well simulated, which is suggested to be caused by the lateral transport of ^{231}Pa from North Atlantic to Southern Ocean by AMOC (Gherardi et al., 2009; Lippold et al., 2011, 2012a; Luo et al., 2010; Rempfer et al., 2017).

The sediment ^{231}Pa/^{230}Th in CTRL is overall consistent with observations (references of observations are listed in Table 3). The North Atlantic shows low sediment ^{231}Pa/^{230}Th activity ratio as in observations because ^{231}Pa is more subject to the southward transport by active ocean circulation than ^{230}Th because of its longer residence time. The Southern Ocean maximum in the sediment ^{231}Pa/^{230}Th activity ratio is also simulated in CTRL. High opal fluxes in the Southern Ocean, which preferentially removes ^{231}Pa into sediment ($K_{opal}^{^{231}Pa} > K_{opal}^{^{230}Th}$) (Chase et al., 2002), leading to increased sediment ^{231}Pa/^{230}Th activity ratio. In addition, upwelling in the Southern Ocean brings up deep water enriched with ^{231}Pa, which is transported from the North Atlantic, to shallower depth and further contribute to the scavenging. CTRL can also produce higher sediment ^{231}Pa/^{230}Th activity ratio in regions with high particle production (e.g. the Eastern equatorial Pacific, the North Pacific and the Indian Ocean) due to the "particle flux effect". Specifically, in North Atlantic, the distribution of sediment ^{231}Pa/^{230}Th matches the distribution of particle, especially opal, production: sediment ^{231}Pa/^{230}Th is higher where opal production is high, and vice versa (Fig. 4 and Fig. 1c).

Deleted: s

Deleted: reasonable

Deleted: tracks

Deleted: southward to the Southern Ocean

4.2 Sensitivity on partition coefficient K

In this section, we show model sensitivity on partition coefficient by increasing and decreasing the partition coefficient, K, by a factor of 5, but keep the relative ratio for different particles the same (Table 2). Our model shows similar model sensitivity as in Siddall et al., (2005) as discussed below.

As stated in Siddall et al., (2005), the isotope decay term in Eq. (3) is three orders of magnitude less than the production term. If we neglect the transport term and the decay term in Eq. (3) and assume particulate phase activity at the surface as 0, when reach equilibrium, the activity of particulate phase will be as in Eq. (7). Eq.(7) combined with Eq.(2) and $R_i = \frac{F}{w_s * \rho}$, we can get Eq.(8). Under the assumption that there is isotope decay and ocean transport, Eq. (7) suggests that the particulate isotope activity depends on the production rate and settling velocity and will increase linearly with depth. Eq. (8) suggests that the dissolved isotope activity depends on the production rate, partition coefficient K and particle flux and will also increase linearly with depth. Any departure from this linear relationship with depth is due to ocean transport, which is suggested by observations (Bacon and Anderson, 1982; Roy-Barman et al., 1996). Results of Eq. (7) and Eq. (8) can help to understand the differences in Exp_1 and Exp_2.

Increasing K will decrease water column dissolved ^{231}Pa and ^{230}Th activities but won't change particulate ^{231}Pa and ^{230}Th too much (Fig. 6). Magnitude of dissolved ^{231}Pa and ^{230}Th in Exp_1 (smaller K) is at least one order larger than that in Exp_2 (larger K), while magnitude of particulate ^{231}Pa and ^{230}Th in Exp_1 and Exp_2 is in the same order. As suggested by Eq. (8), if there is no isotope decay and no ocean transport, larger K will lead to smaller dissolved isotope activity but unchanged particulate activity. Intuitively, larger K will lead to more ^{231}Pa and ^{230}Th attached to particles and further buried into sediment, which increases the sink for the ^{231}Pa and ^{230}Th budget. With the sources for ^{231}Pa and ^{230}Th staying the same, dissolved ^{231}Pa and ^{230}Th will be reduced. Increasing K will also reduce the vertical gradient of dissolved ^{231}Pa and ^{230}Th as reversible scavenging act as the vertical transport and increase this vertical transport can decrease the vertical gradient.

Moved down [2]: Increasing K will decrease water column dissolved ^{231}Pa and ^{230}Th activities but won't change particulate ^{231}Pa and ^{230}Th too much (Fig. 6).

Moved (insertion) [1]

Deleted: a

Moved (insertion) [2]

Deleted: L

However, changes in the particulate ^{231}Pa and ^{230}Th is relatively small (Fig. 6). Eq. (7) suggests that particulate phase activity it is independent of K. Therefore, changing K will have limited influence on particulate phase activity.

$$A_p^i(z) = \frac{\beta^i}{w_s} \cdot z \quad (7)$$

$$A_d^i(z) = \frac{\rho\beta^i}{K^i F} \cdot z \quad (8)$$

Increasing K will also reduce the spatial gradient in sediment ^{231}Pa/^{230}Th activity ratio and vice versa (Fig. 7). Larger K will decrease the ^{231}Pa and ^{230}Th residence time and most isotopes produced in the water column are removed into sediment locally (Table 2). Therefore, sediment ^{231}Pa/^{230}Th ratio becomes more homogeneous and approaching the production ration of 0.093 (Fig. 7b). The deviation (the root mean squared error) of sediment ^{231}Pa/^{230}Th is 0.0726 in CTRL, 0.0770 in Exp_1 and 0.0739 in Exp_2. Together with the water column isotope activity, it suggests that the partition coefficient in CTRL is of the right order of magnitude.

4.3. Sediment ^{231}Pa/^{230}Th ratio in HOSING

Potential changes in the export of biogenic particles makes using ^{231}Pa/^{230}Th ratio to reconstructing AMOC strength under debate. In response to freshwater perturbation in the North Atlantic, both biological productivity and AMOC strength will change and will influence sediment ^{231}Pa/^{230}Th in different ways. Our model with p-fixed and p-coupled ^{231}Pa and ^{230}Th can help to detangle these two effects. In this section, we examine the sediment ^{231}Pa/^{230}Th (p-fixed and p-coupled) response in the North Atlantic to idealized fresh water perturbation.

In HOSING, after applying freshwater forcing to the North Atlantic, AMOC strength quickly decreases to a minimum of 2 Sv (AMOC_off) (Fig. 9a). During the AMOC_off state, compared with CTRL with active AMOC (AMOC_on), p-fixed sediment ^{231}Pa/^{230}Th shows an overall increase in the North Atlantic and a decrease

Deleted: smal

Deleted: l

Moved up [1]: any departure from this linear relationship with depth is due to ocean transport, which is suggested by observations (Bacon and Anderson, 1982; Roy-Barman et al., 1996).

Deleted: As stated in Siddall et al., (2005), if we neglect the transport term and the decay term in Eq. (3) and assume particulate phase activity at the surface as 0, when reach equilibrium, the activity of particulate phase will be as in Eq. (7). The

Deleted: only depends on the production rate, the particle settling velocity and depth

Deleted: The particulate phase activity will increase linearly with depth and

Deleted: The sediment ^{231}Pa/^{230}Th activity ratio in EXP_1 and EXP_2 departures from observations significantly,

Deleted: suggesting

761 in the South Atlantic (Fig. 10b) because of the reduced southward transport of ^{231}Pa
762 from the North Atlantic by AMOC, consistent with paleo proxy evidence there (e.g.
763 Gherardi et al., 2005, 2009; McManus et al., 2004). The overall increase of sediment
764 $^{231}Pa/^{230}Th$ ratio in the North Atlantic in response to the AMOC collapse can be seen
765 more clearly in the time evolution of the sediment $^{231}Pa/^{230}Th$ ratio averaged from
766 20°N to 60°N in the North Atlantic (Fig.9b, green). Quantitatively, the $^{231}Pa/^{230}Th$
767 increases from 0.074 in AMOC_on to 0.098 in AMOC_off in the p-fixed version,
768 approaching the production ration of 0.093. This increase of $^{231}Pa/^{230}Th$ is also in
769 the subtropical North Atlantic from the two sites near Bermuda Rise (Fig. 9e and f),
770 which is of comparable magnitude with the change from LGM to HS1 in
771 reconstructions there (McManus et al., 2004). In addition, the pattern of p-fixed
772 (Fig.10a) sediment $^{231}Pa/^{230}Th$ ratio during the Atlantic in AMOC_off state is similar
773 to the opal distribution (Fig.1b) because, without active circulation, sediment
774 $^{231}Pa/^{230}Th$ ratio is more controlled by particle flux effect, which is similar to the
775 Pacific in CTRL. It is further noted that our p-fixed sediment $^{231}Pa/^{230}Th$ ratio in
776 HOSING behaves similarly to that in Siddall et al., (2007).
777 The overall increase in p-fixed sediment $^{231}Pa/^{230}Th$ ratio in the North
778 Atlantic is not homogenous and the magnitude of the change between AMOC_on and
779 AMOC_off varies with location because of the distribution of particle flux, especially
780 opal flux (Fig.9 and 10). The maximum increase in p-fixed sediment $^{231}Pa/^{230}Th$
781 ratio occurs near 40°N western Atlantic, where the opal production in our model is
782 maximum in North Atlantic (Fig. 1b). It should be noted that the opal maximum in
783 this region is not in the observation (Fig. 7.2.5 in Sarmiento and Gruber 2006).
784 However, our sediment $^{231}Pa/^{230}Th$ response in HOSING is self-consistent with the
785 particle flux in our model. The sediment $^{231}Pa/^{230}Th$ ratio in this region during
786 AMOC_on is larger than production ratio of 0.093 because opal maximum provides
787 extra ^{231}Pa to this region ("particle flux effect"), which overwhelms the active ocean
788 circulation transporting ^{231}Pa southward outside this region (Fig. 9d, green). During
789 AMOC_off, without active ocean circulation, the particle flux effect becomes even
790 stronger because less ^{231}Pa is transported out of the North Atlantic and p-fixed
791 sediment $^{231}Pa/^{230}Th$ ratio gets even larger.

In most regions of the Atlantic, p-coupled sediment $^{231}Pa/^{230}Th$ shows a similar response to p-fixed $^{231}Pa/^{230}Th$ in HOSING. The evolution of p-fixed and p-coupled sediment $^{231}Pa/^{230}Th$ activity ratio in HOSING are highly correlated (Fig. 11a). The change of sediment $^{231}Pa/^{230}Th$ ratio from AMOC_on to AMOC_off are similar in both p-fixed and p-coupled version (Fig.11b). The correlation between p-fixed and p-coupled sediment $^{231}Pa/^{230}Th$ ratio change from AMOC on to AMOC off is 0.72 (1455points) and the linear regression coefficient is 0.71 (R^2 = 0.52). High correlation between p-fixed and p-coupled response mainly happens over low productivity regions (Fig.1, 10, and 11), where circulation effect on sediment $^{231}Pa/^{230}Th$ is more important than the particle flux change in HOSING.

However, the responses of p-fixed and p-coupled sediment $^{231}Pa/^{230}Th$ to the fresh water forcing can differ significantly in high productivity regions because of the importance of the productivity change. With persistent freshwater forcing over the North Atlantic, most regions in the North Atlantic show reduced production of $CaCO_3$, opal and POC (Fig. 8). Productivity in the North Atlantic is suggested to be halved during AMOC collapse because of increased stratification, which reduces nutrient supply from deep ocean (Schmittner, 2005). In our model, the productivity in the mid-latitude North Atlantic is indeed greatly reduced after the freshwater forcing is applied. For example, opal production from 30°N-50°N in the Atlantic at the end of HOSING is reduced by 50%~90% of its original value in CTRL. However, opal production increases in high latitude North Atlantic (north of 50°N). The pattern of opal production changes with high opal production region shifts northward in HOSING (Fig. 8 d, e and f). These particle flux changes will influence sediment $^{231}Pa/^{230}Th$ as discussed below.

North of 50°N in the Atlantic, the opal productivity increases during AMOC_off (Fig. 8f) and will result an increase in sediment $^{231}Pa/^{230}Th$. The increase caused by greater opal productivity enhances the sediment $^{231}Pa/^{230}Th$ increase caused by reduced AMOC. Therefore, the increase in p-coupled sediment $^{231}Pa/^{230}Th$ from AMOC on to AMOC off is larger than p-fixed sediment $^{231}Pa/^{230}Th$ change (Fig.9c).

Deleted: M
Deleted: in
Deleted: change of
Deleted: in
Deleted: at
Deleted: e
Deleted: In subpolar region
Deleted: ,
Deleted: which is enhance the increase of sediment $^{231}Pa/^{230}Th$ caused by reduced AMOC.
Deleted: between
Deleted: off
Deleted: and
Deleted: on

In the mid-latitude North Atlantic, the opal productivity decreases during AMOC_off (Fig.8 f) and will lead to a decrease in sediment $^{231}Pa/^{230}Th$, which is opposite to the effect of reduced AMOC. P-coupled sediment $^{231}Pa/^{230}Th$ shows an initial decrease in first 200 years (Fig.9 d, e, and f, red dash lines) caused by the reduced opal productivity. But this decrease trend is reversed eventually, suggesting that the influence of particle flux change is overwhelmed by the effect of reduced AMOC. It the long run, most regions in the subtropical and mid-latitude Atlantic show increased sediment $^{231}Pa/^{230}Th$ in HOSING (Fig.10 d), indicating the dominant effect of reduced AMOC. However, sediment $^{231}Pa/^{230}Th$ at 40°N west Atlantic, where opal productivity is maximum during AMOC_on, show a decrease from AMOC_on to AMOC_off (Fig.9 d and Fig.10 d). During AMOC_on, the opal productivity maximum at 40°N west Atlantic lead to regional maximum sediment $^{231}Pa/^{230}Th$ because of the particle flux effect (Fig. 4). During AMOC_off, this opal productivity maximum is eliminated (Fig.8 e) and there is no more extra ^{231}Pa supplied by surroundings to this region, which leads to a decrease in sediment $^{231}Pa/^{230}Th$. This decrease in sediment $^{231}Pa/^{230}Th$ caused by productivity change is greater than the increase caused by the reduced AMOC. Therefore, sediment $^{231}Pa/^{230}Th$ experiences a decrease from AMOC_on to AMOC_off at this location (Fig.9 d and Fig.10 d). Our results suggest that although the circulation effect is more dominant than the particle flux change in controlling sediment $^{231}Pa/^{230}Th$ on long time scale over most of North Atlantic (Fig. 11), particle flux change can be important on short time scale and in high productivity regions. With p-fixed and p-coupled ^{231}Pa and ^{230}Th, our model can help to detangle the circulation effect and particle flux effect.

It is suggested that the particulate $^{231}Pa/^{230}Th$ response to the change of AMOC depends on the location and depth. Above 2km and high latitude North Atlantic, particulate $^{231}Pa/^{230}Th$ decreases with the increased AMOC (Rempfer et al., 2017). Our results are consistent with this finding (Fig. 12 a and b). Both p-fixed and p-coupled particulate $^{231}Pa/^{230}Th$ show similar patterns of change from AMOC_on to AMOC_off: decrease in particulate $^{231}Pa/^{230}Th$ at shallow depth and north of 60°N and increase in particulate $^{231}Pa/^{230}Th$ below 2km and south of 60°N during

Deleted: Therefore, p

Deleted:

Deleted: But

Deleted: in

Deleted: ed, which has been explained previously

Deleted: is

Deleted: The

Deleted: larger

Deleted: experienced

Deleted: in

Deleted: and

Formatted: Not Highlight

Formatted: Not Highlight

Deleted: Therefore, we should be cautious when using sediment $^{231}Pa/^{230}Th$ to reconstruct AMOC variations in the past.

Deleted: .

Formatted: Indent: First line: 0"

Deleted: between

Deleted: and

AMOC_off. Therefore, sediment depth should also be taken into consideration when interpreting sediment $^{231}Pa/^{230}Th$. Since the pattern in p-coupled is similar to the pattern in p-fixed, the opposite particulate $^{231}Pa/^{230}Th$ changes in shallow and deep North Atlantic is associated with AMOC change. During AMOC_on, upper limb of AMOC (about upper 1km) transport water northward, which provides extra ^{231}Pa to North Atlantic and particulate $^{231}Pa/^{230}Th$ is larger than the production ratio of 0.093. In contrast, the lower limb of AMOC (2km-3km) features southward transport, which transports ^{231}Pa to the Southern Ocean and particulate $^{231}Pa/^{230}Th$ is smaller than the production ratio of 0.093 (Fig. 12 solid). Particulate $^{231}Pa/^{230}Th$ decreases with depth (Fig. 12 c solid). During AMOC_off, ocean transport of ^{231}Pa is greatly reduced. Therefore, shallow (deep) depth experiences a decrease (increase) in particulate $^{231}Pa/^{230}Th$ and the vertical gradient in the particulate $^{231}Pa/^{230}Th$ is also greatly reduced (Fig. 12 c dash). Our results support that the depth dependence of particulate $^{231}Pa/^{230}Th$ is mainly caused by lateral transport of ^{231}Pa by circulation (Gherardi et al., 2009; Lippold et al., 2011, 2012a; Luo et al., 2010; Rempfer et al., 2017).

Overall, our model is able to simulate the correct magnitude of the sediment $^{231}Pa/^{230}Th$ ratio response to the freshwater forcing. Change of circulation has the dominant influence on sediment $^{231}Pa/^{230}Th$ on long time scale over most of regions in the idealized hosing experiment, although the detailed difference between p-fixed and p-coupled sediment $^{231}Pa/^{230}Th$ ratio response to freshwater forcing in different locations can be complicated.

5. Summary

^{231}Pa and ^{230}Th have been implemented in the ocean model of the CESM in both the p-coupled and p-fixed forms. Our control experiment under present day climate forcing is able to simulate most ^{231}Pa and ^{230}Th water column activity and sediment $^{231}Pa/^{230}Th$ activity ratio consistent with observations by using the parameters that are suggested by Chase et al., (2002) and used in Siddall et al.

Deleted:

Formatted: Superscript

(2005). Our sensitivity experiments with varying parameters suggest that these parameters are of the right order of magnitude.

Furthermore, our model is able to simulate the overall sediment $^{231}Pa/^{230}Th$ ratio change in the North Atlantic with a magnitude comparable to the reconstruction in response to the collapse of AMOC, although the detailed response can be complicated in different regions. Finally, the p-fixed form is able to capture many major features of that of the p-coupled form over large ocean areas on long time scale, although the two forms can also differ significantly in some regions, especially the region with high opal productivity.

However, our implementation of ^{231}Pa and ^{230}Th can be further improved by including nepheloid layers to better simulate water column ^{231}Pa and ^{230}Th activity as in Rempfer et al., 2017. In addition, partition coefficient for different particles can be further tuned in the future, which can improve our understanding of the affinity of ^{231}Pa and ^{230}Th to different particles, complementing the limited observational studies available (e.g. Chase et al., 2002; Scholten et al., 2005; Walter et al., 1997). Nevertheless, as the first attempt to implement ^{231}Pa and ^{230}Th in the CESM with both p-fixed and p-coupled versions, our model can serve as a useful tool to improve our understanding of the processes of ^{231}Pa and ^{230}Th and also interpretations of sediment $^{231}Pa/^{230}Th$ reconstructions for past ocean circulation and climate changes.

Deleted: Therefore, with both p-fixed and p-coupled ^{231}Pa and ^{230}Th, our model can serve as a useful tool to improve our understanding of the processes of ^{231}Pa and ^{230}Th and also interpretations of sediment $^{231}Pa/^{230}Th$ reconstructions for past ocean circulation and climate changes.

Code availability:

The ^{231}Pa and ^{230}Th isotope source code of both p-fixed and p-coupled versions for CESM1.3 is included as supplementary material here.

Acknowledgement:

This work is supported by US NSF P2C2 program (NSF 1401778 and NSF1401802),), DOE DE-SC0006744 and the National Science Foundation of China No. 41630527 and 41130105. Computing resources (ark:/85065/d7wd3xhc) were provided by

Deleted:

the Climate Simulation Laboratory at NCAR's Computational and Information Systems Laboratory, sponsored by the National Science Foundation and other agencies.

References:

Anderson, R. F., Bacon, M. P. and Brewer, P. G.: Removal of230Th and231Pa from the open ocean, Earth Planet. Sci. Lett., 62(1), 7–23, doi:10.1016/0012-821X(83)90067-5, 1983.

Anderson, R. F., Lao, Y., Broecker, W. S., Trumbore, S. E., Hofmann, H. J. and Wolfli, W.: Boundary scavenging in the Pacific Ocean: A comparison of 10Be and 231Pa, Earth Planet. Sci. Lett., 96(3–4), 287–304, doi:10.1016/j.cognition.2008.05.007, 1990.

Anderson, R. F., Fleisher, M. Q., Biscaye, P. E., Kumar, N., Dittrich, B., Kubik, P. and Suter, M.: Anomalous boundary scavenging in the Middle Atlantic Bight: evidence from 230Th, 231Pa, 10Be and 210Pb, Deep. Res. Part II, 41(2–3), 537–561, doi:10.1016/0967-0645(94)90034-5, 1994.

Armstrong, R. A., Lee, C., Hedges, J. I., Honjo, S. and Wakeham, S. G.: A new, mechanistic model for organic carbon fluxes in the ocean based on the quantitative association of POC with ballast minerals, Deep. Res. Part II Top. Stud. Oceanogr., 49(1–3), 219–236, doi:10.1016/S0967-0645(01)00101-1, 2002.

Arsouze, T., Dutay, J.-C., Lacan, F. and Jeandel, C.: Reconstructing the Nd oceanic cycle using a coupled dynamical – biogeochemical model, Biogeosciences, 6(12), 2829–2846, doi:10.5194/bg-6-2829-2009, 2009.

Bacon, M. and Anderson, R.: Distribution of Thorium Isotopes between dissolved and particulate forms in the deep sea, J. Geophys. Res. …, 87(1), 2045–2056, 1982.

Bacon, M. P. and Rosholt, J. N.: Accumulation rates of 230Th, 231Pa, and some transition metals on the Bermuda Rise, Geochim. Cosmochim. Acta, 46, 651–666, 1982.

Bacon, M. P., Huh, C. A. and Moore, R. M.: Vertical profiles of some natural radionuclides over the Alpha Ridge, Arctic Ocean, Earth Planet. Sci. Lett., 95(1–2), 15–22, doi:10.1016/0012-821X(89)90164-7, 1989.

Bradtmiller, L. I., Anderson, R. F., Fleisher, M. Q. and Burckle, L. H.: Opal burial in the equatorial Atlantic Ocean over the last 30 ka: Implications for glacial-interglacial changes in the ocean silicon cycle, Paleoceanography, 22(4), 1–15, doi:10.1029/2007PA001443, 2007.

Bradtmiller, L. I., McManus, J. F. and Robinson, L. F.: 231Pa/230Th evidence for a weakened but persistent Atlantic meridional overturning circulation during Heinrich Stadial 1, Nat. Commun., 5, 5817, doi:10.1038/ncomms6817, 2014.

Burckel, P., Waelbroeck, C., Luo, Y., Roche, D. M., Pichat, S., Jaccard, S. L., Gherardi, J., Govin, A., Lippold, J. and Thil, F.: Changes in the geometry and strength of the Atlantic meridional overturning circulation during the last glacial (20-50 ka), Clim. Past, 12(11), 2061–2075, doi:10.5194/cp-12-2061-2016, 2016.

Chase, Z. and Robert F, A.: Comment on “On the importance of opal, carbonate, and lithogenic clays in scavenging and fractionating 230Th, 231Pa and 10Be in the ocean”

by S. Luo and T.-L. Ku, Earth Planet. Sci. Lett., 220(1–2), 201–211, doi:10.1016/S0012-821X(04)00027-5, 2004.
Chase, Z., Anderson, R. F., Fleisher, M. Q. and Kubik, P. W.: The influence of particle composition and particle flux on scavenging of Th , Pa and Be in the ocean, Earth Planet. Sci. Lett., 204(1–2), 215–229, doi:10.1016/S0012-821X(02)00984-6, 2002.
Cochran, J. K., Livingston, H. D., Hirschberg, D. J. and Surprenant, L. D.: Natural and anthropogenic radionuclide distributions in the northwest Atlantic Ocean, Earth Planet. Sci. Lett., 84(2–3), 135–152, doi:10.1016/0012-821X(87)90081-1, 1987.
Cochran, J. K., Hirschberg, D. J., Livingston, H. D., Buesseler, K. O. and Key, R. M.: Natural and anthropogenic radionuclide distributions in the Nansen Basin, Artic Ocean: Scavenging rates and circulation timescales, Deep. Res. Part II, 42(6), 1495–1517, doi:10.1016/0967-0645(95)00051-8, 1995.
Colley, S., Thomson, J. and Newton, P. P.: Detailed Th-230, Th-232 and Pb-210 fluxes recorded by the 1989/90 BOFS sediment trap time-series at 48N, 20W, Deep - Sea Res. Part I - Oceanogr. Res. Pap., 42(6), 833–848, 1995.
Coppola, L., Roy-Barman, M., Mulsow, S., Povinec, P. and Jeandel, C.: Thorium isotopes as tracers of particles dynamics and deep water circulation in the Indian sector of the Southern Ocean (ANTARES IV), Mar. Chem., 100(3–4 SPEC. ISS.), 299–313, doi:10.1016/j.marchem.2005.10.019, 2006.
Danabasoglu, G., Bates, S. C., Briegleb, B. P., Jayne, S. R., Jochum, M., Large, W. G., Peacock, S. and Yeager, S. G.: The CCSM4 ocean component, J. Clim., 25(5), 1361–1389, doi:10.1175/JCLI-D-11-00091.1, 2012.
DeMaster, D. J.: The marine budgets of silica and 32Si, Yale., 1979.
Deng, F., Thomas, A. L., Rijkenberg, M. J. A. and Henderson, G. M.: Controls on seawater 231Pa, 230Th and 232Th concentrations along the flow paths of deep waters in the Southwest Atlantic, Earth Planet. Sci. Lett., 390, 93–102, doi:10.1016/j.epsl.2013.12.038, 2014.
Doney, S. C., Lima, I., Feely, R. A., Glover, D. M., Lindsay, K., Mahowald, N., Moore, J. K. and Wanninkhof, R.: Mechanisms governing interannual variability in upper-ocean inorganic carbon system and air-sea CO2 fluxes: Physical climate and atmospheric dust, Deep. Res. Part II Top. Stud. Oceanogr., 56(8–10), 640–655, doi:10.1016/j.dsr2.2008.12.006, 2009.
Dutay, J.-C., Lacan, F., Roy-Barman, M. and Bopp, L.: Influence of particle size and type on 231 Pa and 230 Th simulation with a global coupled biogeochemical-ocean general circulation model: A first approach, Geochemistry, Geophys. Geosystems, 10(1), doi:10.1029/2008GC002291, 2009.
Edmonds, H. N., Moran, S. B., Hoff, J. A., Smith, J. N. and Edwards, R. L.: Protactinium-231 and Thorium-230 Abundances and High Scavenging Rates in the Western Arctic Ocean, Science (80-.)., 280(5362), 405–407, doi:10.1126/science.280.5362.405, 1998.
Edmonds, H. N., Moran, S. B., Cheng, H. and Edwards, R. L.: 230Th and 231Pa in the Arctic Ocean: Implications for particle fluxes and basin-scale Th/Pa fractionation, Earth Planet. Sci. Lett., 227(1–2), 155–167, doi:10.1016/j.epsl.2004.08.008, 2004.
Francois, R., Bacon, M. P., Altabet, M. A. and Labeyrie, L. D.: Glacial/interglacial changes in sediment rain rate in the SW Indian Sector of subantarctic Waters as recorded by 230Th, 231Pa, U, and d15N, Paleoceanography, 8(5), 611–629,

doi:10.1029/93PA00784, 1993.
Frank, M.: Reconstruction of Late Quaternary environmental conditions applying the natural radionuclides 230Th, 10Be, 231Pa and 238U: A study of deep-sea sediments from the eastern sector of the Antarctic Circumpolar Current System, Alfred Wegener Institute for Polar and Marine Research., 1996.
Frank, M., Eisenhauer, A., Kubik, P. W., Dittrich-hannen, B. and Segl, M.: Beryllium 10, thorium 230, and protactinium 231 in Galapagos microplate sediments: Implications of hydrothermal activity and paleoproductivity changes during the last 100,000 years, Palaeogeography, 9(4), 559–578, 1994.
Geibert, W. and Usbeck, R.: Adsorption of thorium and protactinium onto different particle types: Experimental findings, Geochim. Cosmochim. Acta, 68(7), 1489–1501, doi:10.1016/j.gca.2003.10.011, 2004.
Gherardi, J., Labeyrie, L., Mcmanus, J., Francois, R., Skinner, L. and Cortijo, E.: Evidence from the Northeastern Atlantic basin for variability in the rate of the meridional overturning circulation through the last deglaciation, Earth Planet. Sci. Lett., 240(3–4), 710–723, doi:10.1016/j.epsl.2005.09.061, 2005.
Gherardi, J.-M., Labeyrie, L., Nave, S., Francois, R., McManus, J. F. and Cortijo, E.: Glacial-interglacial circulation changes inferred from 231 Pa/ 230 Th sedimentary record in the North Atlantic region, Paleoceanography, 24(2), doi:10.1029/2008PA001696, 2009.
Gu, S., Liu, Z., Zhang, J., Rempfer, J., Joos, J., Brady, E. and Oppo, D.: Coherent response of Antarctic Intermediate Water and Atlantic Meridional Overturning Circulation during the last deglaciation, Palaeogeography, doi:10.1002/2017PA003092, 2017.
Guo, L., Santschi, P. H., Baskaran, M. and Zindler, A.: Distribution of dissolved and particulate 230Th and 232Th in seawater from the Gulf of Mexico and off Cape Hatteras as measured by SIMS, Earth Planet. Sci. Lett., 133(1), 117–128, 1995.
Gutjahr, M., Frank, M., Stirling, C. H., Keigwin, L. D. and Halliday, a. N.: Tracing the Nd isotope evolution of North Atlantic Deep and Intermediate Waters in the western North Atlantic since the Last Glacial Maximum from Blake Ridge sediments, Earth Planet. Sci. Lett., 266(1–2), 61–77, doi:10.1016/j.epsl.2007.10.037, 2008.
Hall, I. R., Moran, S. B., Zahn, R., Knutz, P. C., Shen, C.-C. and Edwards, R. L.: Accelerated drawdown of meridional overturning in the late-glacial Atlantic triggered by transient pre-H event freshwater perturbation, Geophys. Res. Lett., 33(16), L16616, doi:10.1029/2006GL026239, 2006.
Hayes, C. T., Anderson, R. F., Fleisher, M. Q., Serno, S., Winckler, G. and Gersonde, R.: Quantifying lithogenic inputs to the North Pacific Ocean using the long-lived thorium isotopes, Earth Planet. Sci. Lett., 383, 16–25, doi:10.1016/j.epsl.2013.09.025, 2013.
Hayes, C. T., Anderson, R. F., Fleisher, M. Q., Huang, K. F., Robinson, L. F., Lu, Y., Cheng, H., Edwards, R. L. and Moran, S. B.: ^{230}Th and ^{231}Pa on GEOTRACES GA03, the U.S. GEOTRACES North Atlantic transect, and implications for modern and paleoceanographic chemical fluxes, Deep. Res. Part II Top. Stud. Oceanogr., 116, 29–41, doi:10.1016/j.dsr2.2014.07.007, 2015.
Henderson, G. M. and Anderson, R. F.: The U-series toolbox for paleoceanography, Rev. Mineral. Geochemistry, 52(1), 493–531, doi:10.2113/0520493, 2003.
Henderson, G. M., Heinze, C., Anderson, R. F. and Winguth, A. M. E.: Global

distribution of the 230Th flux to ocean sediments constrained by GCM modelling, Deep. Res. Part I Oceanogr. Res. Pap., 46(11), 1861–1893, doi:10.1016/S0967-0637(99)00030-8, 1999.
Hoffmann, S. S., McManus, J. F., Curry, W. B. and Brown-Leger, L. S.: Persistent export of 231Pa from the deep central Arctic Ocean over the past 35,000 years., Nature, 497(7451), 603–6, doi:10.1038/nature12145, 2013.
Hsieh, Y. Te, Henderson, G. M. and Thomas, A. L.: Combining seawater 232Th and 230Th concentrations to determine dust fluxes to the surface ocean, Earth Planet. Sci. Lett., 312(3–4), 280–290, doi:10.1016/j.epsl.2011.10.022, 2011.
Huh, C. A. and Beasley, T. M.: Profiles of dissolved and particulate thorium isotopes in the water column of coastal Southern California, Earth Planet. Sci. Lett., 85(1–3), 1–10, doi:10.1016/0012-821X(87)90016-1, 1987.
Hurrell, J. W., Holland, M. M., Gent, P. R., Ghan, S., Kay, J. E., Kushner, P. J., Lamarque, J. F., Large, W. G., Lawrence, D., Lindsay, K., Lipscomb, W. H., Long, M. C., Mahowald, N., Marsh, D. R., Neale, R. B., Rasch, P., Vavrus, S., Vertenstein, M., Bader, D., Collins, W. D., Hack, J. J., Kiehl, J. and Marshall, S.: The community earth system model: A framework for collaborative research, Bull. Am. Meteorol. Soc., 94(9), 1339–1360, doi:10.1175/BAMS-D-12-00121.1, 2013.
Jahn, A., Lindsay, K., Giraud, X., Gruber, N., Otto-Bliesner, B. L., Liu, Z. and Brady, E. C.: Carbon isotopes in the ocean model of the Community Earth System Model (CESM1), Geosci. Model Dev., 8(8), 2419–2434, doi:10.5194/gmd-8-2419-2015, 2015.
Jonkers, L., Zahn, R., Thomas, A., Henderson, G., Abouchami, W., Fran??ois, R., Masque, P., Hall, I. R. and Bickert, T.: Deep circulation changes in the central South Atlantic during the past 145 kyrs reflected in a combined 231Pa/230Th, Neodymium isotope and benthic dC13 record, Earth Planet. Sci. Lett., 419, 14–21, doi:10.1016/j.epsl.2015.03.004, 2015.
Keigwin, L. D. and Boyle, E. A.: Did North Atlantic overturning halt 17,000 years ago?, Paleoceanography, 23(1), 1–5, doi:10.1029/2007PA001500, 2008.
Kriest, I.: Different parameterizations of marine snow in a 1D-model and their influence on representation of marine snow, nitrogen budget and sedimentation, Deep. Res. Part I Oceanogr. Res. Pap., 49(12), 2133–2162, doi:10.1016/S0967-0637(02)00127-9, 2002.
Ku, T. L.: Uranium series disequilibrium in deep sea sediments, Columbia., 1966.
Ku, T. L., Bischoff, J. L. and Boersma, A.: Age studies of Mid-Atlantic Ridge sediments near 42??N and 20??N, Deep. Res. Oceanogr. Abstr., 19(3), 233–247, doi:10.1016/0011-7471(72)90033-2, 1972.
Kumar, N.: Trace metals and natural radionuclides as tracers of ocean productivity, Columbia., 1994.
Kumar, N., Gwiazda, R., Anderson, R. F. and Froelich, P. N.: 231Pa/230Th ratios in sediments as a proxy for past changes in Southern Ocean productivity, Nature, 362, 45–48, doi:10.1038/362045a0, 1993.
Large, W. G. and Yeager, S. G.: The global climatology of an interannually varying air–sea flux data set, Clim. Dyn., 33(2–3), 341–364, doi:10.1007/s00382-008-0441-3, 2008.
Lippold, J., Grützner, J., Winter, D., Lahaye, Y., Mangini, A. and Christi, M.: Does sedimentary 231Pa/230Th from the Bermuda Rise monitor past Atlantic Meridional

Overturning Circulation?, Geophys. Res. Lett., 36(12), 1–6, doi:10.1029/2009GL038068, 2009.
Lippold, J., Gherardi, J. M. and Luo, Y.: Testing the $^{231}Pa/^{230}Th$ paleocirculation proxy: A data versus 2D model comparison, Geophys. Res. Lett., 38(20), 1–7, doi:10.1029/2011GL049282, 2011.
Lippold, J., Mulitza, S., Mollenhauer, G., Weyer, S., Heslop, D. and Christl, M.: Boundary scavenging at the East Atlantic margin does not negate use of 231Pa/230Th to trace Atlantic overturning, Earth Planet. Sci. Lett., 333–334, 317–331, doi:10.1016/j.epsl.2012.04.005, 2012a.
Lippold, J., Luo, Y., Francois, R., Allen, S. E., Gherardi, J., Pichat, S., Hickey, B. and Schulz, H.: Strength and geometry of the glacial Atlantic Meridional Overturning Circulation, Nat. Geosci., 5(11), 813–816, doi:10.1038/ngeo1608, 2012b.
Long, M. C., Lindsay, K., Peacock, S., Moore, J. K. and Doney, S. C.: Twentieth-century oceanic carbon uptake and storage in CESM1(BGC), J. Clim., 26(18), 6775–6800, doi:10.1175/JCLI-D-12-00184.s1, 2013.
Luo, S. and Ku, T. L.: Oceanic 231Pa/230Th ratio influenced by particle composition and remineralization, Earth Planet. Sci. Lett., 167(3–4), 183–195, doi:10.1016/S0012-821X(99)00035-7, 1999.
Luo, S. D., Ku, T. L., Kusakabe, M., Bishop, J. K. B. and Yang, Y. L.: Tracing particle cycling in the upper ocean with Th-230 and Th-228: An investigation in the equatorial Pacific along 140 degrees W, Deep - Sea Res. Part II - Top. Stud. Oceanogr., 42(2–3), 805–829, doi:10.1016/0967-0645(95)00019-M, 1995.
Luo, Y., Francois, R. and Allen, S.: Sediment 231Pa/230Th as a recorder of the rate of the Atlantic meridional overturning circulation: insights from a 2-D model, Ocean Sci., 6(3), 381–400, doi:10.5194/os-6-381-2010, 2010.
Mangini, A. and Diester-Hass, L.: Excess Th-230 in sediments off NW Africa traces upwelling during the past 130,000 years, in Coastal upwelling: Its sedimentary records, edited by E. Suess and J. Thiede, pp. 455–470, Plenum., 1983.
Mangini, A. and Key, R. M.: A 230Th profile in the Atlantic Ocean, Earth Planet. Sci. Lett., 62(3), 377–384, doi:10.1016/0012-821X(83)90008-0, 1983.
Mangini, A. and Sonntag, C.: 231Pa dating of deep-sea cores via 227Th counting, Earth Planet. Sci. Lett., 37(2), 251–256, 1977.
Mangini, A. and U., K.: Depositional history in the Clarion-Clipperton zone during the last 250,000 years: 230Th and 231Pa methods, Geol. Jahrb., 87, 105–121, 1987.
Marchal, O., François, R., Stocker, T. F. and Joos, F.: Ocean thermohaline circulation and sedimentary 231Pa/230Th ratio, Paleoceanography, 15(6), 625–641 [online] Available from: http://onlinelibrary.wiley.com/doi/10.1029/2000PA000496/full (Accessed 19 April 2016), 2000.
McManus, J., Francois, R. and Gherardi, J.: Collapse and rapid resumption of Atlantic meridional circulation linked to deglacial climate changes, Nature, 428(6985), 834–837, 2004.
Moore, J. K. and Braucher, O.: Sedimentary and mineral dust sources of dissolved iron to the World Ocean, Biogeosciences, 5(1994), 631–656, doi:10.5194/bgd-4-1279-2007, 2008.
Moore, J. K., Doney, S. C., Glover, D. M. and Fung, I. Y.: Iron cycling and nutrient-limitation patterns in surface waters of the World Ocean, , 49, 463–507, 2002.

Moore, J. K., Doney, S. C. and Lindsay, K.: Upper ocean ecosystem dynamics and iron cycling in a global three-dimensional model, Global Biogeochem. Cycles, 18(4), doi:10.1029/2004GB002220, 2004.
Moore, J. K., Lindsay, K., Doney, S. C., Long, M. C. and Misumi, K.: Marine Ecosystem Dynamics and Biogeochemical Cycling in the Community Earth System Model [CESM1(BGC)]: Comparison of the 1990s with the 2090s under the RCP4.5 and RCP8.5 Scenarios, J. Clim., 26(23), 9291–9312, doi:10.1175/JCLI-D-12-00566.1, 2013.
Moore, R. M. and Hunter, K. A.: Thorium adsorption in the ocean: reversibility and distribution amongst particle sizes, Geochim. Cosmochim. Acta, 49(11), 2253–2257, doi:10.1016/0016-7037(85)90225-X, 1985.
Moore, W. S.: The thorium isotope content of ocean water, Earth Planet. Sci. Lett., 53(3), 419–426, doi:10.1016/0012-821X(81)90046-7, 1981.
Moran, S. B., Hoff, J. A., Buesseler, K. O. and Edwards, R. L.: High precision 230Th and 232Th in the Norwegian Sea and Denmark by thermal ionization mass spectrometry, , 22(19), 2589–2592, 1995.
Moran, S. B., Charette, M. a., Hoff, J. a., Edwards, R. L. and Landing, W. M.: Distribution of 230Th in the Labrador Sea and its relation to ventilation, Earth Planet. Sci. Lett., 150, 151–160, doi:10.1016/S0012-821X(97)00081-2, 1997.
Moran, S. B., Shen, C.-C., Weinstein, S. E., Hettinger, L. H., Hoff, J. H., E dmonds, H. N. and Edwards, R. L.: Constraints on deep water age and particle flux in the Equatorial and South Atlantic Ocean based on seawater 231Pa and 230Th data, Geophys. Res. Lett., 28(18), 3437–3440 [online] Available from: papers2://publication/uuid/2A811583-B32B-4BD8-B582-EC8B0D96A949, 2001.
Moran, S. B., Shen, C. C., Edmonds, H. N., Weinstein, S. E., Smith, J. N. and Edwards, R. L.: Dissolved and particulate 231Pa and 230Th in the Atlantic Ocean: Constraints on intermediate/deep water age, boundary scavenging, and 231Pa/230Th fractionation, Earth Planet. Sci. Lett., 203(3–4), 999–1014, doi:10.1016/S0012-821X(02)00928-7, 2002.
Müller, P. J. and Mangini, A.: Organic carbon decomposition rates in sediments of the pacific manganese nodule belt dated by 230Th and 231Pa, Earth Planet. Sci. Lett., 51(1), 94–114, doi:10.1016/0012-821X(80)90259-9, 1980.
Negre, C., Zahn, R., Thomas, A. L., Masqué, P., Henderson, G. M., Martínez-Méndez, G., Hall, I. R. and Mas, J. L.: Reversed flow of Atlantic deep water during the Last Glacial Maximum., Nature, 468(7320), 84–88, doi:10.1038/nature09508, 2010.
Nozaki, Y. and Horibe, Y.: Alpha-emitting thorium isotopes in northwest Pacific deep waters, Earth Planet. Sci. Lett., 65(1), 39–50, doi:10.1016/0012-821X(83)90188-7, 1983.
Nozaki, Y. and Nakanishi, T.: 231Pa and 230Th profiles in the open ocean water column, Deep Sea Res. Part A, Oceanogr. Res. Pap., 32(10), 1209–1220, doi:10.1016/0198-0149(85)90004-4, 1985.
Nozaki, Y. and Yamada, M.: Thorium and protactinium isotope distributions in waters of the Japan Sea, Deep Sea Res. Part A, Oceanogr. Res. Pap., 34(8), 1417–1430, 1987.
Nozaki, Y. and Yang, H. S.: Th and Pa isotopes in the waters of the western margin of the pacific near Japan: Evidence for release of228Ra and227Ac from slope

sediments, J. Oceanogr. Soc. Japan, 43(4), 217–227, doi:10.1007/BF02109817, 1987.
Nozaki, Y., Horibe, Y. and Tsubota, H.: The water column distribution of thorium isotopes in the western North Pacific, Earth Planet. Sci. Lett., 54(54), 203–216, 1981.
Nozaki, Y., Yang, H.-S. and Yamada, M.: Scavenging of thorium in the ocean, J. Geophys. Res., 92(C1), 772, doi:10.1029/JC092iC01p00772, 1987.
Okubo, A., Obata, H., Nozaki, Y., Yamamoto, Y. and Minami, H.: 230Th in the Andaman Sea: Rapid deep-sea renewal, Geophys. Res. Lett., 31(22), 1–5, doi:10.1029/2004GL020226, 2004.
Okubo, A., Obata, H., Luo, S., Gamo, T., Yamamoto, Y., Minami, H. and Yamada, M.: Particle flux in the twilight zone of the eastern Indian Ocean: A constraint from 234U-230Th and 228Ra-228Th disequilibria, Deep. Res. Part I Oceanogr. Res. Pap., 54(10), 1758–1772, doi:10.1016/j.dsr.2007.06.009, 2007a.
Okubo, A., Obata, H., Gamo, T., Minami, H. and Yamada, M.: Scavenging of 230Th in the Sulu Sea, Deep. Res. Part II Top. Stud. Oceanogr., 54(1–2), 50–59, doi:10.1016/j.dsr2.2006.02.016, 2007b.
Okubo, A., Obata, H., Gamo, T. and Yamada, M.: 230Th and 232Th distributions in mid-latitudes of the North Pacific Ocean: Effect of bottom scavenging, Earth Planet. Sci. Lett., 339–340, 139–150, doi:10.1016/j.epsl.2012.05.012, 2012.
Rempfer, J., Stocker, T. F., Joos, F., Lippold, J. and Jaccard, S. L.: New insights into cycling of 231 Pa and 230 Th in the Atlantic Ocean, Earth Planet. Sci. Lett., 468, 27–37, doi:10.1016/j.epsl.2017.03.027, 2017.
Roberts, N. L., McManus, J. F., Piotrowski, A. M. and McCave, I. N.: Advection and scavenging controls of Pa/Th in the northern NE Atlantic, Paleoceanography, 29(6), 668–679, doi:10.1002/2014PA002633, 2014.
Robinson, L. F., Belshaw, N. S. and Henderson, G. M.: U and Th concentrations and isotope ratios in modern carbonates and waters from the Bahamas, Geochim. Cosmochim. Acta, 68(8), 1777–1789, doi:10.1016/j.gca.2003.10.005, 2004.
Roy-Barman, M., Chen, J. H. and Wasserburg, G. J.: 230Th-232Th systematics in the central Pacific Ocean: The sources and the fates of thorium, Earth Planet. Sci. Lett., 139(3–4), 351–363, doi:10.1016/0012-821X(96)00017-9, 1996.
Rutgers van der Loeff, M. M. and Berger, G. W.: Scavenging of 230Th and 231Pa near the antarctic polar front in the South Atlantic, Deep. Res. Part I, 40(2), 339–357, doi:10.1016/0967-0637(93)90007-P, 1993.
Schmittner, A.: Decline of the marine ecosystem caused by a reduction in the Atlantic overturning circulation., Nature, 434(7033), 628–633, doi:10.1038/nature03476, 2005.
Schmitz, W., Mangini, A., Stoffers, P., Glasby, G. P. and Pluger, W. L.: Sediment accumulation rates in the southwestern Pacific Basin and Aitutaki Passage, Mar. Geol., 73(1), 181–190, 1986.
Scholten, J. C., Rutgers van der Loeff, M. M. and Michel, A.: Distribution of 230Th and 231Pa in the water column in relation to the ventilation of the deep Arctic basins, Deep. Res. Part II, 42(6), 1519–1531, doi:10.1016/0967-0645(95)00052-6, 1995.
Scholten, J. C., Fietzke, J., Mangini, A., Stoffers, P., Rixen, T., Gaye-Haake, B., Blanz, T., Ramaswamy, V., Sirocko, F., Schulz, H. and Ittekkot, V.: Radionuclide fluxes in the Arabian Sea: The role of particle composition, Earth Planet. Sci. Lett., 230(3–4), 319–337, doi:10.1016/j.epsl.2004.11.003, 2005.

Scholten, J. C., Fietzke, J., Mangini, A., Garbe-Schönberg, C. D., Eisenhauer, A., Schneider, R. and Stoffers, P.: Advection and scavenging: Effects on 230Th and 231Pa distribution off Southwest Africa, Earth Planet. Sci. Lett., 271(1–4), 159–169, doi:10.1016/j.epsl.2008.03.060, 2008.
Shimmield, G. B. and Price, N. B.: The scavenging of U,230Th and 231Pa during pulsed hydrothermal activity at 20??S, East Pacific Rise, Geochim. Cosmochim. Acta, 52(3), 669–677, doi:10.1016/0016-7037(88)90329-8, 1988.
Shimmield, G. B., Murray, J. W., Thomson, J., Bacon, M. P., Anderson, R. F. and Price, N. B.: The distribution and behaviour of 230Th and 231Pa at an ocean margin, Baja California, Mexico, Geochim. Cosmochim. Acta, 50(11), 2499–2507, doi:10.1016/0016-7037(86)90032-3, 1986.
Siddall, M., Henderson, G. M., Edwards, N. R., Frank, M., Müller, S. a., Stocker, T. F. and Joos, F.: 231Pa/230Th fractionation by ocean transport, biogenic particle flux and particle type, Earth Planet. Sci. Lett., 237(1–2), 135–155, doi:10.1016/j.epsl.2005.05.031, 2005.
Siddall, M., Stocker, T. F., Henderson, G. M., Joos, F., Frank, M., Edwards, N. R., Ritz, S. P. and Müller, S. a.: Modeling the relationship between 231 Pa/ 230 Th distribution in North Atlantic sediment and Atlantic meridional overturning circulation, Paleoceanography, 22(2), n/a-n/a, doi:10.1029/2006PA001358, 2007.
Thomas, A. L., Henderson, G. M. and Robinson, L. F.: Interpretation of the 231Pa/230Th paleocirculation proxy: New water-column measurements from the southwest Indian Ocean, Earth Planet. Sci. Lett., 241(3–4), 493–504, doi:10.1016/j.epsl.2005.11.031, 2006.
Trimble, S. M., Baskaran, M. and Porcelli, D.: Scavenging of thorium isotopes in the Canada Basin of the Arctic Ocean, Earth Planet. Sci. Lett., 222(3–4), 915–932, doi:10.1016/j.epsl.2004.03.027, 2004.
Venchiarutti, C., van der Loeff, M. R. and Stimac, I.: Scavenging of 231Pa and thorium isotopes based on dissolved and size-fractionated particulate distributions at Drake Passage (ANTXXIV-3), Deep. Res. Part II Top. Stud. Oceanogr., 58(25–26), 2767–2784, doi:10.1016/j.dsr2.2010.10.040, 2011.
Vogler, S., Scholten, J., Rutgers van der Loeff, M. M. and Mangini, A.: 230Th in the eastern North Atlantic: the importance of water mass ventilation in the balance of 230Th, Earth Planet. Sci. Lett., 156(1–2), 61–74, doi:10.1016/S0012-821X(98)00011-9, 1998.
Walter, H. J., Rutgers van der Loeff, M. M. and Hoeltzen, H.: Enhanced scavenging of 231Pa relative to 230Th in the South Atlantic south of the Polar Front: Implications for the use of the 231Pa/230Th ratio as a paleoproductivity proxy, Earth Planet. Sci. Lett., 149(1), 85–100, doi:10.1016/S0012-821X(97)00068-X, 1997.
Yang, H. S., Nozaki, Y., Sakai, H. and Masuda, A.: The distribution of 230Th and 231Pa in the deep-sea surface sediments of the Pacific Ocean, Geochim. Cosmochim. Acta, 50(1), 81–89, doi:10.1016/0016-7037(86)90050-5, 1986.
Yong-Liang Yang, Elderfield, H., Pedersen, T. F. and Ivanovich, M.: Geochemical record of the Panama Basin during the Last Glacial Maximum carbon event shows that the glacial ocean was not suboxic, Geology, 23(12), 1115–1118, doi:10.1130/0091-7613(1995)023<1115:GROTPB>2.3.CO, 1995.
Yong Lao, Anderson, R. F., Broecker, W. S., Trumbore, S. E., Hofmann, H. J. and Wolfli,

W.: Transport and burial rates of 10Be and 231Pa in the Pacific Ocean during the Holocene period, Earth Planet. Sci. Lett., 113(1–2), 173–189, doi:10.1016/0012-821X(92)90218-K, 1992.
Yu, E.-F.: Variations in the Particulate Flux of 230Th and 231Pa and Paleoceanographic Applications of the 231Pa/230Th Ratio, WHOI/MIT., 1994.
Yu, E.-F., Francois, R. and Bacon, M. P.: Similar rates of modern and last-glacial ocean thermohaline circulation inferred from radiochemical data, Nature, 379(6567), 689–694, doi:10.1038/379689a0, 1996.

Variable	Symbol	Value	Units
Production of ^{231}Pa from U decay	β^{Pa}	2.33*10^{-3}	dpm m^{-3} yr^{-1}
Production of ^{230}Th from U decay	β^{Th}	2.52*10^{-2}	dpm m^{-3} yr^{-1}
Decay constant of ^{231}Pa	λ^{Pa}	2.13*10^{-5}	yr^{-1}
Decay constant of ^{230}Th	λ^{Th}	9.22*10^{-6}	yr^{-1}
Index for ^{231}Pa and ^{230}Th	i		
Index for particle type	j		
Total isotope activity	A_t		dpm m^{-3}
Dissolved isotope activity	A_d		dpm m^{-3}
Particle associated activity	A_p		dpm m^{-3}
Particle settling velocity	w_s	1000	m yr^{-1}
Particle concentration	C		kg m^{-3}
Density of seawater		1024.5	kg m^{-3}
Ratio between particle concentration and density of seawater	R		

Table 1. List of parameters, abbreviations and values.

	CTRL		EXP_1		EXP_2	
	^{231}Pa	^{230}Th	^{231}Pa	^{230}Th	^{231}Pa	^{230}Th
K_{CaCO_3}	2.5*10^5	1.0*10^7	5*10^4	2*10^6	1.25*10^6	5*10^7
K_{opal}	1.67*10^6	5*10^5	3.33*10^5	1*10^5	8.33*10^6	2.5*10^6
K_{POC}	1.0*10^7	1.0*10^7	2*10^6	2*10^6	5*10^7	5*10^7
τ (yr)	118	33	501	143	27	9

Deleted: T

Table 2. Partition coefficients for different particle types and residence time for ^{231}Pa and ^{230}Th in different experiments. Partition coefficients used in CTRL follows (Chase et al., 2002; Siddall et al., 2005). Both p-coupled and p-fixed versions are enabled in CTRL, which yields identical results (discussed in section 4.1). Only p-fixed version is enabled in Exp_1 and Exp_2. The residence time (τ) is for p-fixed version in each experiment.

WATER COLUMN ACTIVITY	**Holocene core-top ^{231}Pa/^{230}Th**
(Guo et al., 1995)	(Yu, 1994)
(Cochran et al., 1987)	(DeMaster, 1979)
(Nozaki et al., 1987)	(Bacon and Rosholt, 1982)
(Bacon and Anderson, 1982)	(Mangini and Diester-Hass, 1983)
(Bacon et al., 1989)	(Kumar, 1994)

Formatted: Font:Bold

Formatted Table

(Huh and Beasley, 1987),	(Yang et al., 1986),
(Rutgers van der Loeff and Berger, 1993)	(Anderson et al., 1983)
(Nozaki et al., 1981)	(Anderson et al., 1994)
(Nozaki and Nakanishi, 1985)	(Ku, 1966)
(Mangini and Key, 1983)	(Ku et al., 1972)
(Nozaki and Horibe, 1983)	(Frank et al., 1994)
(Moore, 1981)	(Shimmield et al., 1986)
(Nozaki and Yamada, 1987)	(Frank, 1996)
(Roy-Barman et al., 1996)	(Yong Lao et al., 1992)
(Nozaki and Yang, 1987)	(Francois et al., 1993)
(Moran et al., 1995)	(Anderson et al., 1990)
(Luo et al., 1995)	(Mangini and Sonntag, 1977)
(Colley et al., 1995)	(Schmitz et al., 1986)
(Scholten et al., 1995)	(Shimmield and Price, 1988)
(Cochran et al., 1995)	(Yong-Liang Yang et al., 1995)
(Vogler et al., 1998)	(Müller and Mangini, 1980)
(Moran et al., 1997)	(Mangini and U., 1987)
(Edmonds et al., 1998)	(Scholten et al., 1995)
(Moran et al., 2001)	(Walter et al., 1997)
(Edmonds et al., 2004)	(Lippold et al., 2011)
(Okubo et al., 2007b)	(Lippold et al., 2012b)
(Coppola et al., 2006)	(Bradtmiller et al., 2007)
(Moran et al., 2002)	(Gherardi et al., 2005)
(Okubo et al., 2004)	(Gutjahr et al., 2008)
(Okubo et al., 2007a)	(Hall et al., 2006)
(Okubo et al., 2012)	(Lippold et al., 2011)
(Robinson et al., 2004)	(Roberts et al., 2014)
(Thomas et al., 2006)	(Bradtmiller et al., 2014)
(Trimble et al., 2004)	(Burckel et al., 2016)
(Venchiarutti et al., 2011)	(Hoffmann et al., 2013)
(Hsieh et al., 2011)	(Jonkers et al., 2015)
(Scholten et al., 2008)	(Negre et al., 2010)
(Luo et al., 2010),	
(Deng et al., 2014)	
(Hayes et al., 2013)	
(Hayes et al., 2015)	

Table 3. References for observations of water column ^{231}Pa and ^{230}Th activity and Holocene core-top $^{231}Pa/^{230}Th$.

Deleted: ... [2]

Deleted: ... [3]

Formatted Table

Deleted: ... [4]

Figures:

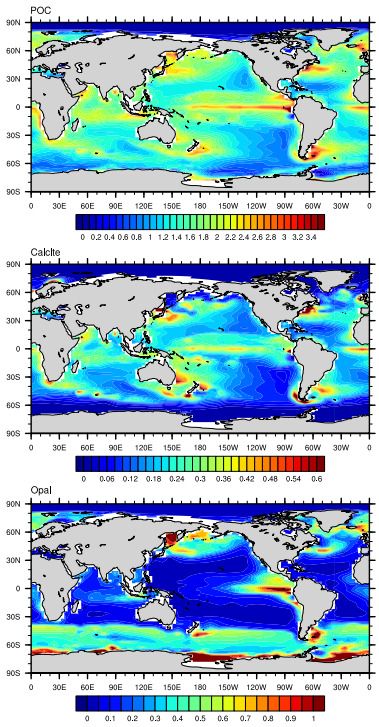

Figure 1. Annual mean particle fluxes in CESM. (a) $CaCO_3$ flux at 105m (mol m^{-2} yr^{-1}). (b) Opal flux at 105m (mol m^{-2} yr^{-1}). (c) POC flux at 105m (mol m^{-2} yr^{-1}).

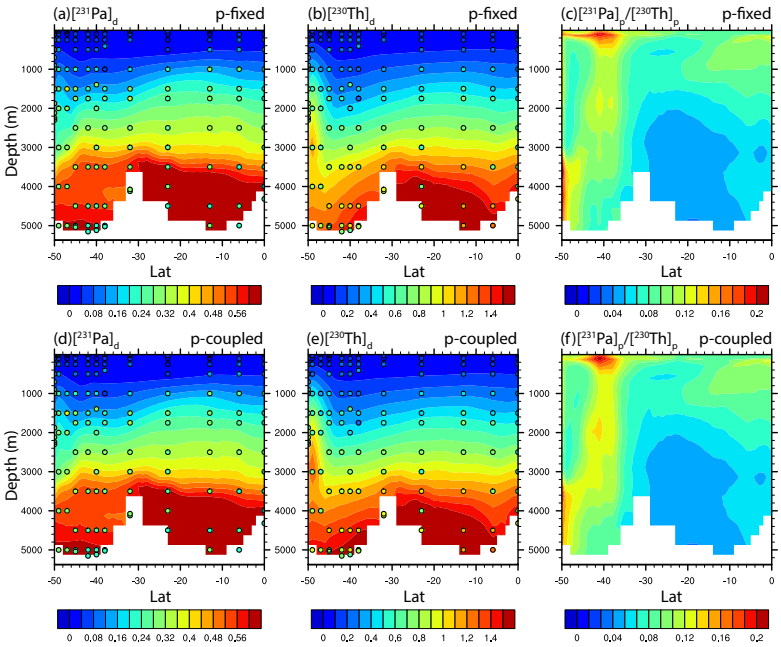

Figure 2. Dissolved ^{231}Pa, dissolved ^{230}Th and particulate ^{231}Pa/^{230}Th in CTRL along GEOTRACES transect GA02S (Deng et al., 2014) (the track is indicated in Fig. S4) for both p-fixed and p-coupled ^{231}Pa and ^{230}Th. Observations of dissolved ^{231}Pa and ^{230}Th activity are superimposed using the same colormap.

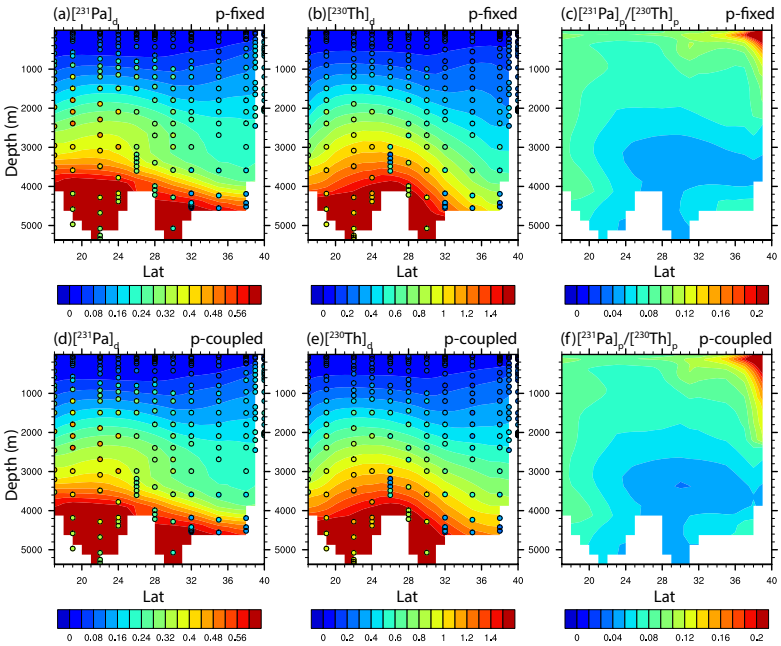

1381

1382 Figure 3. Dissolved ^{231}Pa, dissolved ^{230}Th and particulate ^{231}Pa/^{230}Th in CTRL along
1383 GEOTRACES transect GA03 (Hayes et al., 2015) (the track is indicated in Fig. S4) for
1384 both p-fixed and p-coupled ^{231}Pa and ^{230}Th. Observations of dissolved ^{231}Pa and
1385 ^{230}Th activity are superimposed using the same colormap.

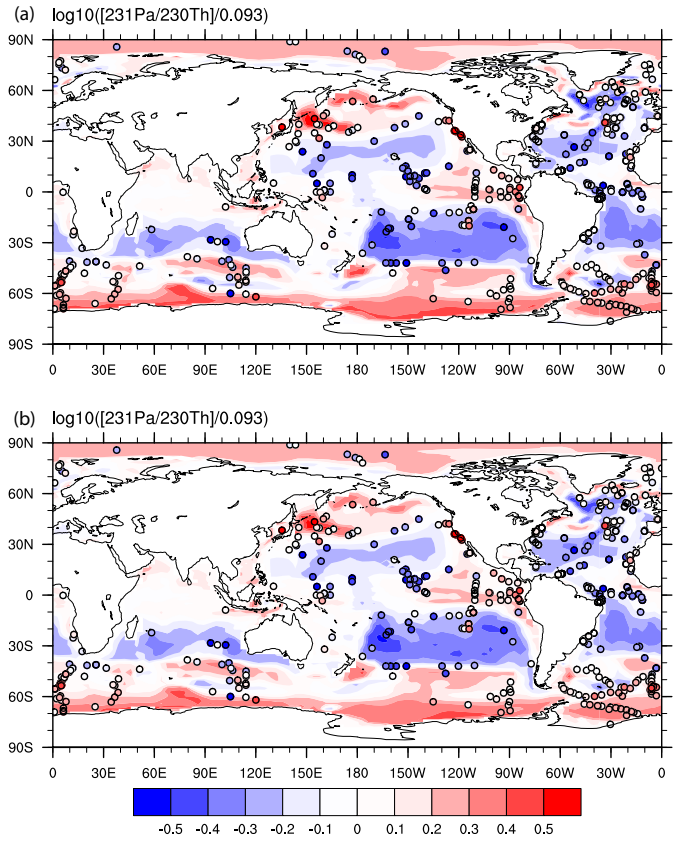

Figure 4. Sediment $^{231}Pa/^{230}Th$ activity ratio in CTRL for both p-fixed (a) and p-coupled version (b). Observations are attached as filled cycles using the same color map. The $^{231}Pa/^{230}Th$ activity ratio is plotted relative to the production ratio of 0.093 on a $\log_{10}$ scale.

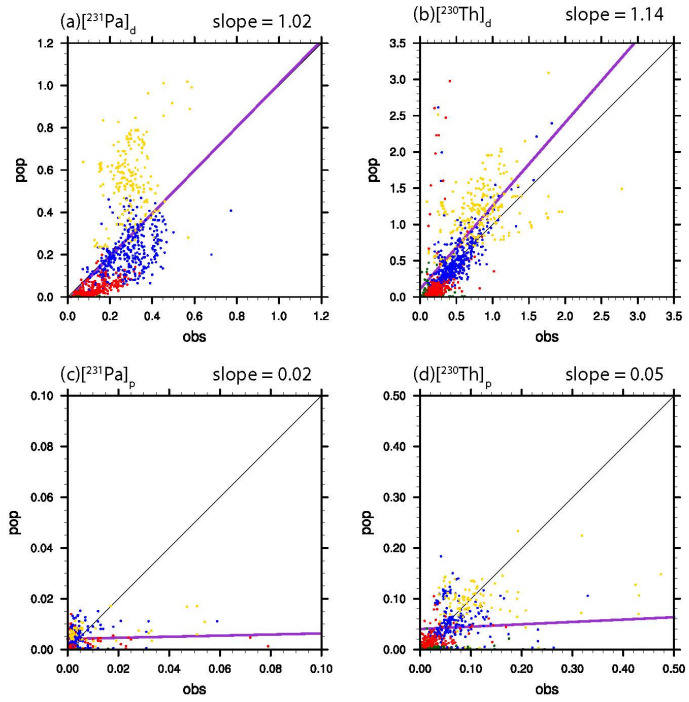

Figure 5. Scatter plot of global dissolved and particulate ^{231}Pa and ^{230}Th between observation and CTRL (p-fixed) (unit: dpm/m^3). (a) dissolved ^{231}Pa; (b) particulate ^{231}Pa; (c) dissolved ^{230}Th; (d) particulate ^{230}Th. Observations in different depth range are indicated by different colors: green for 0-100m; red for 100m-1000m; blue for 1000m-3000m and yellow for deeper than 3000m. Purple line is the least squared linear regression line and slope is the linear regression coefficient.

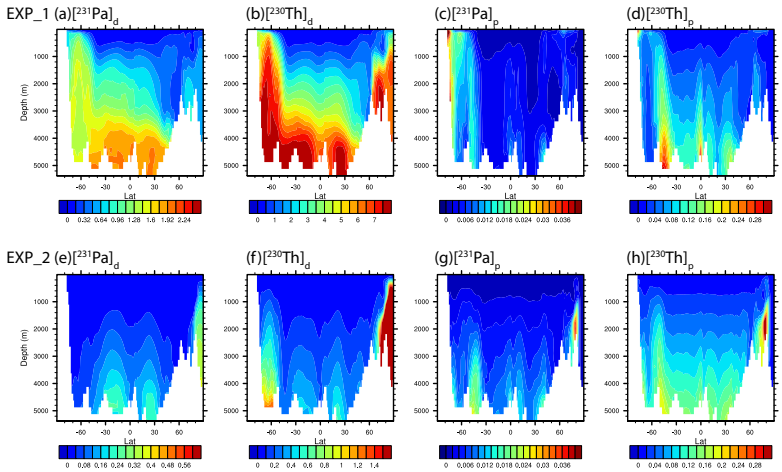

Figure 6. Atlantic zonal mean dissolved and particulate ^{231}Pa and ^{230}Th in EXP_1 and EXP_2 (unit: dpm/m^3). EXP_1: (a) dissolved ^{231}Pa; (b) dissolved ^{230}Th; (c) particulate ^{231}Pa; (d) particulate ^{230}Th. EXP_2: (e) dissolved ^{231}Pa; (f) dissolved ^{230}Th; (g) particulate ^{231}Pa; (h) particulate ^{230}Th.

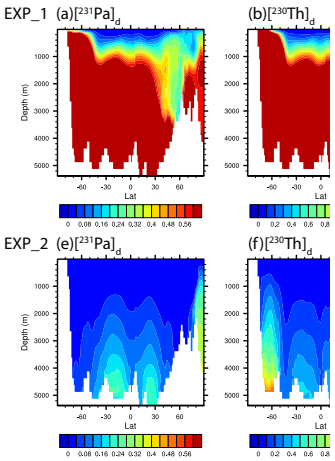

Deleted:

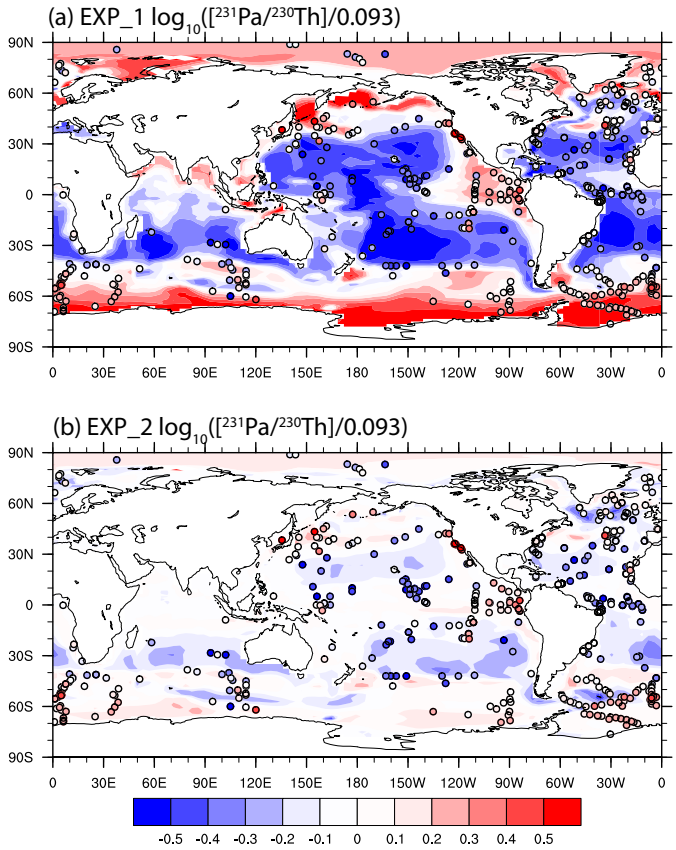

1409

1410 Figure 7. Sediment $^{231}Pa/^{230}Th$ activity ratio in EXP_1 (a) and EXP_2 (b).
1411 Observations are attached as filled cycles using the same color map. The $^{231}Pa/^{230}Th$
1412 activity ratio is plotted relative to the production ratio of 0.093 on a $\log_{10}$ scale.

1413

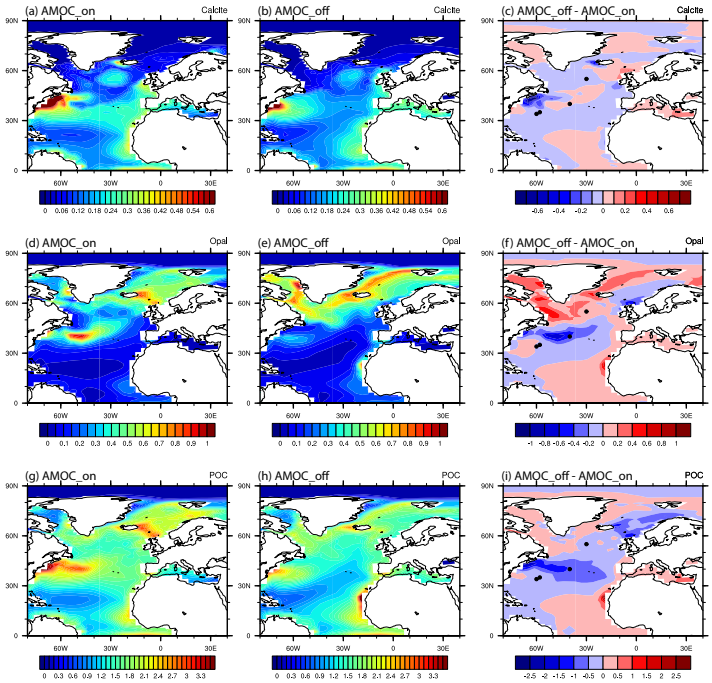

Figure 8. Comparison of particle fluxes between AMOC_on and AMOC_off. $CaCO_3$ flux at 105m (mol m^{-2} yr^{-1}) during AMOC_on (a), AMOC_off (b) and difference between AMOC_off and AMOC_on. (b) Opal flux at 105m (mol m^{-2} yr^{-1}) during AMOC_on (d), AMOC_off (e) and difference between AMOC_off and AMOC_on (f). POC flux at 105m (mol m^{-2} yr^{-1}) during AMOC_on (g), AMOC_off (h) and difference between AMOC_off and AMOC_on (i).

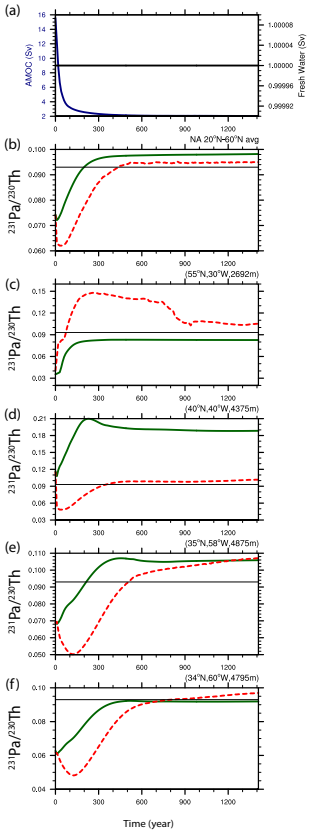

Figure 9. Time evolutions in HOSING. (a) Freshwater forcing (black) and AMOC strength (navy), which is defined as the maximum of the overturning streamfunction below 500m in the North Atlantic. (b) North Atlantic average sediment $^{231}Pa/^{230}Th$ activity ratio from 20°N to 60°N: p-fixed (green) and p-coupled (red). Production ratio of 0.093 is indicated by a solid black line (similar in c, d, e and f). (c) Sediment $^{231}Pa/^{230}Th$ activity ratio at (55°N, 30°W). (d) Sediment $^{231}Pa/^{230}Th$ activity ratio at (40°N, 40°W). (e) Sediment $^{231}Pa/^{230}Th$ activity ratio at (35°N, 58°W). (f) Sediment $^{231}Pa/^{230}Th$ activity ratio at (34°N, 60°W). (e) and (f) are near Bermuda Rise. Locations of each site are shown as dots in Fig. 8b.

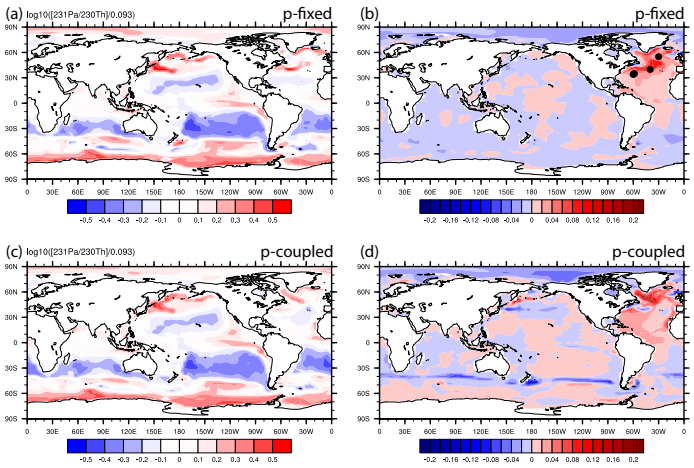

Figure 10. Sediment $^{231}Pa/^{230}Th$ activity ratio during AMOC off state and the difference between AMOC off and CTRL. (a) P-fixed $\log_{10}([^{231}Pa/^{230}Th]/0.093)$ in AMOC_off. (b) Difference of p-fixed sediment $^{231}Pa/^{230}Th$ activity ratio between AMOC_off and AMOC_on. (c) and (d) are similar to (a) and (b) for p-coupled sediment $^{231}Pa/^{230}Th$ activity ratio. Black dots in (b) shows the locations of sites in Fig. 9 from North to South.

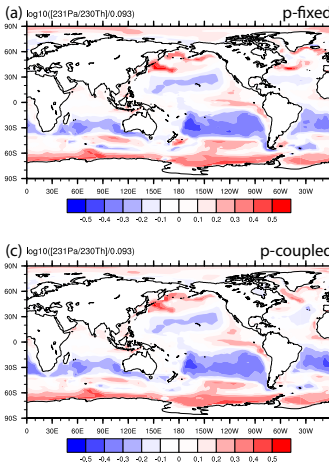

Deleted:

Deleted: 7

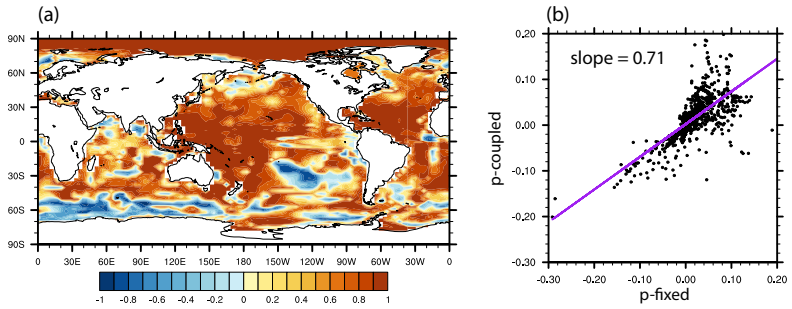

Figure 11. (a) Correlation of p-fixed and p-coupled evolution of sediment $^{231}Pa/^{230}Th$ activity ratio in HOSING. (b) Scatter plot of p-fixed and p-coupled sediment $^{231}Pa/^{230}Th$ activity ratio change from AMOC_on to AMOC_off in the Atlantic and the Southern Ocean (70°W-20°E). Purple line is the least squared linear regression line and slope is the linear regression coefficient.

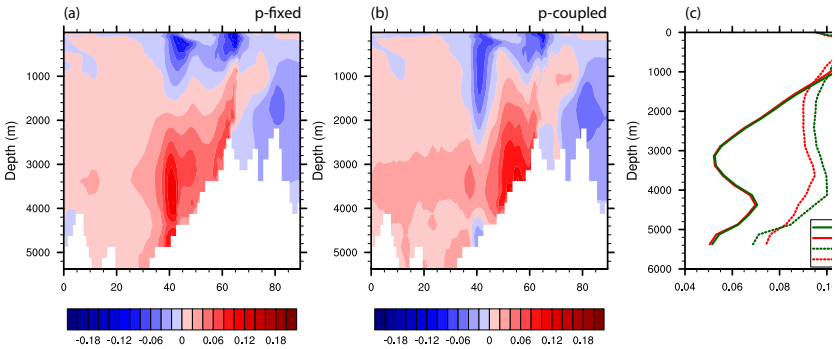

Figure 12. Difference of Atlantic zonal mean particulate $^{231}Pa/^{230}Th$ between AMOC_off and AMOC_on: (a) p-fixed and (b) p-coupled. (c) North Atlantic (20°N-60°N) average profile during AMOC_on (solid) and AMOC_off (dash) for p-fixed (green) and p-coupled (red) particulate $^{231}Pa/^{230}Th$.

1458
1459
1460
1461

Page 9: [1] Deleted	Sifan Gu	10/18/17 10:43:00 AM

Page 36: [2] Deleted	Sifan Gu	10/10/17 4:07:00 PM

(Rutgers van der Loeff and Berger, 1993)
(Nozaki et al., 1981)

Page 36: [3] Deleted	Sifan Gu	10/10/17 4:07:00 PM

(Anderson et al., 1983)
(Anderson et al., 1994)

Page 36: [4] Deleted	Sifan Gu	10/10/17 4:04:00 PM

(Deng et al., 2014)
(Hayes et al., 2013)
(Hayes et al., 2015)